frontiers | Frontiers in Earth Science

ORIGINAL RESEARCH
published: 27 June 2022
doi: 10.3389/feart.2022.880003

The Northernmost Volcanoes in South America (Colombia, 5–6°N): The Potentially Active Samaná Monogenetic Volcanic Field

Laura Sánchez-Torres[1,2]*, *Hugo Murcia*[2,3] *and Dayana Schonwalder-Ángel*[4]

[1]*Maestría en Ciencias de la Tierra, Universidad de Caldas, Manizales, Colombia,* [2]*Instituto de Investigaciones en Estratigrafía (IIES), Universidad de Caldas, Manizales, Colombia,* [3]*Departamento de Ciencias Geológicas, Universidad de Caldas, Manizales, Colombia,* [4]*Estancia Posdoctoral, MINCIENCIAS-Universidad de Caldas, Manizales, Colombia*

The northernmost volcanism in South America (5–6°N) is defined by the presence of several monogenetic volcanic edifices in Colombia, which have been grouped within the Samaná monogenetic volcanic field. Few volcanoes have been studied so far, but they are recognized as a cluster of volcanoes of intermediate-to-acid composition, formed by both explosive and effusive eruptions. This study aims to 1) characterize four more monogenetic volcanic edifices as part of the Samaná field, 2) highlight the potentially active volcanism in an area previously defined as non-volcanogenic, and 3) give insights into the magmatic evolution of the scarcely studied evolved monogenetic volcanism linked to subduction zones worldwide. To achieve these aims, this study uses petrography, mineral chemistry, whole-rock geochemistry, geochronological analyses, and geothermobarometric calculations. The analyses indicate that the field is formed by at least seven volcanoes with similar composition and that it is long-lived and potentially active. Mineralogically, the erupted products host plagioclase ($An_{26–74}$) and amphibole (magnesio-hastingsite, tschermakite, and occasionally mangesio-hornblende) as the most abundant phases, although orthopyroxene (enstatite; $Wo_{2–3}$, $En_{70–76}$, $Fs_{21–28}$) and clinopyroxene (diopside and augite; $Wo_{44–45}$, $En_{41–42}$, $Fs_{13–15}$, and $Wo_{42–44}$, $En_{46–47}$, $Fs_{10–11}$) also appear. Less abundant phases such as olivine ($Fo_{81–88}$), biotite (magnesiobiotite), quartz, and Fe–Ti oxides ($Usp_{4–89}$ $Mag_{96–11}$, and $Ilm_{61–92}$ $Hem_{39–8}$) were also recognized. Chemically, the volcanoes are of andesitic-to-dacitic composition with calc-alkaline affinity and show similar behavior of LILE, HFSE, and REE, which is typical for magmatism in subduction environments. Ages yield a range between 1.32 ± 0.06 Ma (K/Ar) and 16,919 ± 220 years (^{14}C). The results also indicate that the volcanoes share a common magmatic source that fed the individual eruptions and that the magma differentiation is mainly controlled by processes of fractional crystallization, although evidence of magma recharge processes or magma mixing and assimilation as a minor process are also recognized. Geothermobarometric calculations suggest that the different mineral phases are crystallized between 1,194 and 687 °C and a pressure between 0.88 and 0.19 GPa. This indicates that the aforementioned processes occurred not only at the main magmatic reservoir (~33–21 km depth) but also at different stagnation zones at shallower levels of the

OPEN ACCESS

Edited by:
Karoly Nemeth,
Massey University, New Zealand

Reviewed by:
Anna O. Volynets,
Far Eastern Branch (RAS), Russia
Tamás Sági,
Eötvös Loránd University, Hungary

****Correspondence:***
Laura Sánchez-Torres
lsancheztorres15@gmail.com

Specialty section:
This article was submitted to Volcanology, a section of the journal Frontiers in Earth Science

Received: *20 February 2022*
Accepted: *13 May 2022*
Published: *27 June 2022*

Citation:
Sánchez-Torres L, Murcia H and Schonwalder-Ángel D (2022) The Northernmost Volcanoes in South America (Colombia, 5–6°N): The Potentially Active Samaná Monogenetic Volcanic Field. Front. Earth Sci. 10:880003. doi: 10.3389/feart.2022.880003

crust (~7–5 km). Taking this into account, it is shown that the magma evolution of this monogenetic field is more complex than individual batches of magma reaching the surface uninterrupted, as is normally described for monogenetic volcanic fields of more mafic compositions in other tectonic settings.

Keywords: silicic monogenetic volcanism, effusive monogenetic eruptions, magma stagnation, long-lived monogenetic fields, complex magma evolution

1 INTRODUCTION

A monogenetic volcanic field is a group of monogenetic volcanoes concentrated in a region on the Earth´s surface (Németh, 2010; Cañón-Tapia, 2016; Smith & Németh, 2017). These fields represent the most common magmatic systems on Earth, occurring in all tectonic settings, although they are less common in subduction environments (Cañón-Tapia, 2016; McGee & Smith, 2016; Smith & Németh, 2017). Monogenetic volcanoes are formed by small volumes of magma (generally $<1\ km^3$) that erupt only once, typically with basaltic compositions, as a result of a rapid magma ascent without significant pauses in the path to the surface (Valentine & Gregg, 2008). Less common are eruptions of intermediate-to-evolved magma batches that evidence evolution linked to stagnation en route and therefore processes of fractional crystallization, assimilation, and sometimes magma recharge and mixing (Rapprich et al., 2017; Murcia & Németh, 2020). Nowadays, it is recognized that the same monogenetic field can host volcanic landforms associated with both mafic and felsic products and that they might evidence different eruptive styles varying between explosive and effusive eruptions (Boivin & Thouret, 2014; Murcia et al., 2019; Sosa-Ceballos et al., 2021; Valentine et al., 2021).

The northernmost volcanism in the South American Andes (5–6°N) is related to the subduction of the Nazca plate under the South American plate (e.g. Monsalve-Bustamante, 2020). It is represented by a recently identified monogenetic volcanic field, which is characterized by having bimodal eruptive style (i.e., explosive and effusive) and evolved compositions (up to SiO_2 = 69 wt.%) (Murcia et al., 2019). There, only the San Diego maar (Borrero et al., 2017), the El Escondido tuff cone (Monsalve et al., 2019; Sánchez-Torres et al., 2019), and the Pela Huevos dome (Sánchez-Torres et al., 2019) have been clearly recognized as volcanoes and therefore previously studied. This work characterizes four more monogenetic volcanic edifices (Norcasia, Piamonte, Morrón, and Guadalupe) as part of the Samaná Monogenetic Volcanic Field (SMVF), highlights the potentially active volcanism in an area previously defined as non-volcanogenic (Vargas & Mann, 2013; Syracuse et al., 2016; Mora et al., 2017; Wagner et al., 2017), and sheds light into the magmatic evolution of the scarcely studied evolved monogenetic volcanism in subduction zones around the globe (Murcia & Németh, 2020).

This article geologically characterizes the SMVF through petrography, mineral chemistry, whole-rock, and geochronological analyses and uses these results to 1) identify magmatic processes through mineral textures, 2) define the crystallization conditions of the identified mineral assemblages, and 3) evaluate the magma evolution in the volcanic field. Thus, this work intends to take a first step in the identification on this type of volcanism in the area and, therefore, open the possibility for future and more in-depth research.

2 GEOLOGICAL BACKGROUND

The San Diego—Cerro Machín Volcano-Tectonic Province (SCVTP), where the SMVF is located (**Figures 1A,B**), is a volcanic chain with a complex tectonic history. To the northwest, it is linked to collision of the Chocó-Panamá microplate and the low subduction angle of the oceanic Caribbean plate under the continental South American plate (Suter et al., 2008; Vargas & Mann, 2013; Idárraga-Garcia et al., 2016). To the west, the Nazca plate subducts under the South American plate (Taboada et al., 2000; Cediel et al., 2003; Cortés et al., 2005), and it seems to be divided into two segments with different subduction angles (Pennington, 1981), associated with a weakness zone generated by the Sandra Ridge prolongation (Lonsdale, 2005) to the east. This weakness crosses underneath the SMVF (**Figure 1A**) and is known as the Caldas Tear (Vargas & Mann, 2013). The prolongation of this tear to the surface has been defined as the limit of the volcanism given by the boundary marked between a "normal" subduction (volcanogenic) to the south and a "flat" subduction (non-volcanogenic) to the north (Vargas & Mann, 2013; Syracuse et al., 2016; Mora et al., 2017; Wagner et al., 2017). However, Londoño et al. (2020), based on the recently reported volcanism north of the Caldas Tear (Borrero et al., 2017; Monsalve et al., 2019; Murcia et al., 2019; Sánchez-Torres et al., 2019), proposed to move this volcanic limit from 5 to 6°N. Structurally, this tectonic setting has developed two main fault systems in the area: a NE–SW fault system (**Figure 1C**), which corresponds to strike–slip faults with right lateral movement as a result of stresses linked to convergence between the Nazca and South American plates (Cortés et al., 2005), and a NW–SE direction fault system (**Figure 1C**), which corresponds to normal faults, some with left lateral movement, associated with the collision of the Chocó-Panamá block (Bohórquez et al., 2005; Suter et al., 2008).

In the region, the boundaries between the crust and mantle and lithosphere and asthenosphere have been proposed at 45 and 105 km, respectively (Murcia et al., 2019). The SMVF is emplaced over the Triassic (Villagómez et al., 2011) or Upper Jurassic (Blanco-Quintero et al., 2014) metamorphic rocks of the Cajamarca Complex, the Triassic San Diego Gneissic Intrusive, the Cretaceous Samaná Igneous Complex (Barrero

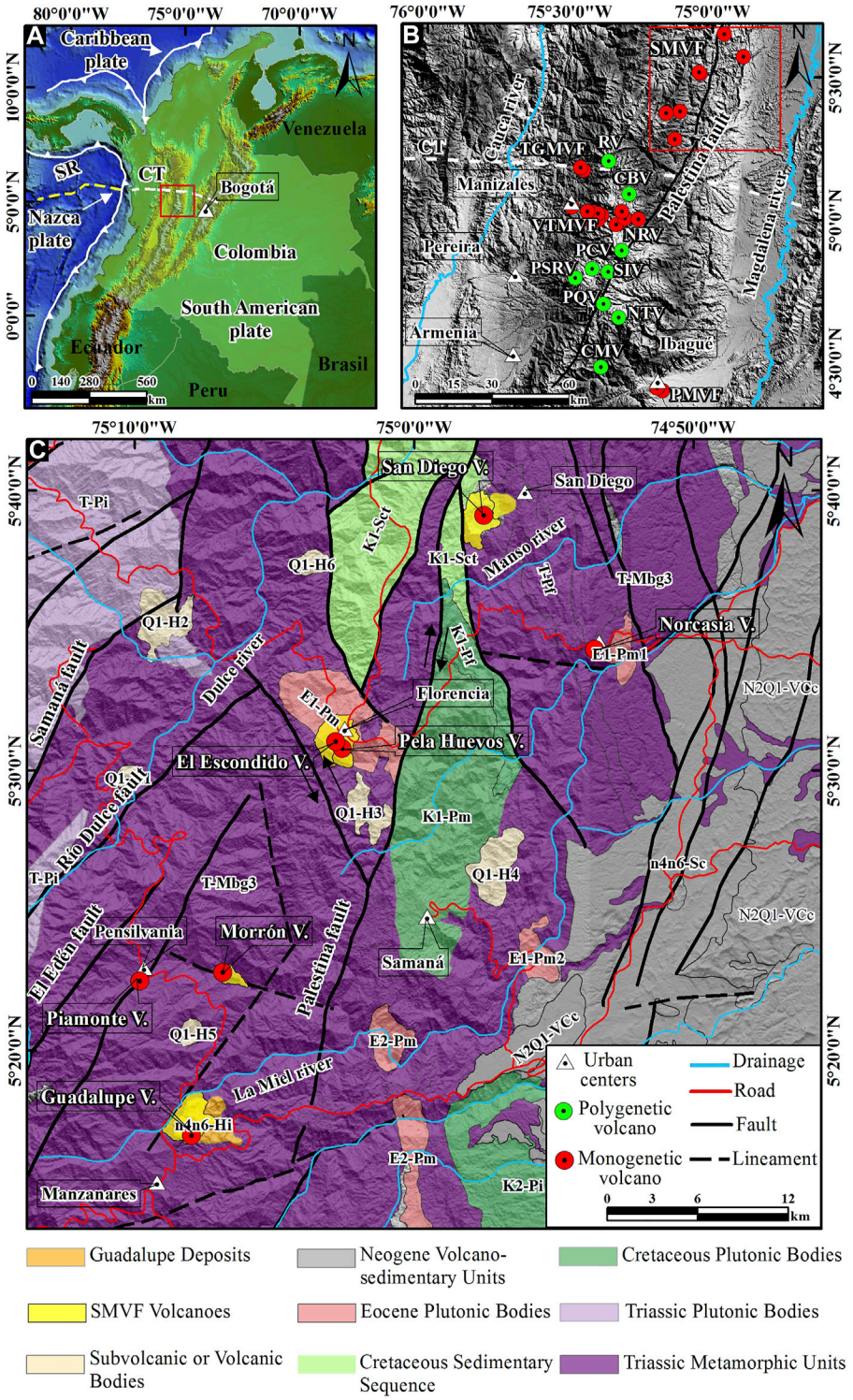

FIGURE 1 | Location maps. **(A)** Location of Colombia in northern South America. **(B)** Digital elevation model illustrating the volcanoes that form the San Diego—Cerro Machín Volcano-Tectonic Province. **(C)** Geological map of Samaná monogenetic volcanic field (Adapted from Gómez-Tapias et al., 2015). SR, Sandra Ridge (yellow dotted line); CT, Caldas Tear (white dotted line); SMFV, Samaná monogenetic volcanic field; TGMVF, Tapias—Guacaica monogenetic volcanic field; VTMVF, Villamaría—Termales monogenetic volcanic field; PMVF, Pijaos monogenetic volcanic field; RV, Romeral volcano; CBV, Cerro Bravo volcano; NRV, Nevado del Ruiz volcano; SIV, Santa Isabel volcano; PCV, Paramillo del Cisne volcano; PSRV, Paramillo de Santa Rosa volcano; PQV, Paramillo del Quindio volcano; NTV, Nevado del Tolima volcano; CMV, Cerro Machín volcano. Geological units: T-Mbg3, Cajamarca Complex; T-Pf, San Diego Gneissic Intrusive; T-Pi, Sonsón

(*Continued*)

FIGURE 1 | Batholith; K1-Pm, Samaná Igneous Complex; K1-Pf, Samaná Alaskite; K2-Pi, Mariquita Stock; K1-Sct, sedimentary sequence; E1-Pm2; La Miel Stock; E1-Pm1, Norcasia Stock; E1-Pm, Florencia Stock; E2-Pm, El Hatillo Stock; n4n6-Sc, Honda Group; N2Q1-Vcc, Mesa Formation; Q1-H1, Río Dulce; Q1-H2, Puente Linda; Q1-H3, Cerro Florencia; Q1-H4, El Morro; Q1-H5, El Alambrado; Q1-H6, La Cabaña; and n4n6-Hi, Guadalupe deposits.

& Vesga, 1976), and a Cretaceous Sedimentary Sequence with no formal name (Gómez-Tapias et al., 2015) (**Figure 1C**). A series of Eocene plutonic bodies have also been recognized (Barrero & Vesga, 1976) (**Figure 1C**). In addition, igneous bodies in the area have been mapped as hornblende-phyric andesitic subvolcanic bodies, which may correspond to other undefined volcanoes (they are known as Río Dulce Puente Linda, Cerro Florencia, El Morro, El Alambrado, and La Cabaña igneous bodies) (**Figure 1C**). This rock type is widely overlain by ash layers, formally defined as Tefra Amarilla (yellow tephra) by Borrero et al. (2017), although the unit has not been mapped, and thus its source is unknown.

2.1 Samaná Monogenetic Volcanic Field

Seven volcanoes have been recognized so far in the SMVF, which covers an area of ~400 km^2. Three of them have known ages, and four are of unknown age. The former are 1) San Diego volcano (**Figure 2A**), a maar formed 20 ka ago and a lava dome to the NE of the maar, which records the last stage of the eruption (Borrero et al., 2017). The maar has an elongated crater (2.1 × 1.5 km in diameter) and hosts a ~50-m-deep lake; its deposits are recognized as dilute pyroclastic density currents formed by phreatic and phreatomagmatic activity, distributed mainly toward the NE side of the volcano (Borrero et al., 2017). 2) El Escondido volcano (**Figure 2B**), a 38-ka tuff cone (Sánchez-Torres et al., 2019); it presents a semi-circular crater (~1.7 km diameter) and flanks with slopes between 10 and 15°. El Escondido deposits are distributed toward the N and E sides of the volcano and records a spectrum of concentrated and dilute pyroclastic density currents and secondary deposits formed by both magmatic and phreatomagmatic activities (Sánchez-Torres et al., 2019). 3) Pela Huevos volcano (**Figure 2C**), a 154-ka lava dome, 250 m high with an elongated conical shape (Rueda-Gutiérrez, 2019); it is located on the SE limit of El Escondido volcano and was disrupted by the eruption that formed the El Escondido volcano (Sánchez-Torres et al., 2019). The volcanoes of unknown age are 4) Piamonte volcano (**Figure 2D**), a ~220-m-high lava dome with a conical shape, flat at the top, 5) Morrón volcano (**Figure 2E**), a 350-m-high lava dome with a conical morphology, elongated toward E, 6) Guadalupe volcano (**Figure 2F**), a lava dome with a conical morphology and volcaniclastic deposits (block and ash pyroclastic flow deposits) around it, and 7) Norcasia volcano (**Figure 2G**) defined by volcaniclastic products without a clear morphology.

3 MATERIALS AND METHODS

3.1 Petrography and Mineral Chemistry

Nine samples were collected from the seven studied volcanoes (**Table 1**). Thin sections were made in Teclab laboratories (Colombia). The petrographic analysis was carried out by point counting in each section, using a Nikon Eclipse E200 petrographic microscope. The size of phenocrysts was defined as >0.5 mm, that of microphenocrysts between 0.5 and 0.05 mm, and that of microlites (groundmass) <0.05 mm (González, 2008). Mineral chemistry analyses (591) were performed using a JXA-8530F field emission electron probe microanalyzer (FE-EPMA) equipped with five wavelength-dispersive spectrometers, at the Facility for Analysis, Characterization, Testing, and Simulation (FACTS) in Nanyang Technological University (NTU), Singapore. Point analyses were acquired using a focused beam at a probe current of 20 nA and an accelerating voltage of 15 kV for all minerals. Current was reduced to 10 nA and defocused beam diameters of 3 and 10 μm for analysis of plagioclase and glass, respectively. The results were quantified using well-characterized natural and synthetic external calibration standards and a ZAF matrix correction procedure. The standards used were T1-G for Si and Al, P&H block Geo MkII for Ca (wollastonite), Ti (rutile), Mg (periclase), K (orthoclase), Fe (specularite), Mn (rhodonite), and P (apatite), and Astimex block MINM25-53 for Na (albite). The oxygen content was assumed from cation abundance, with all iron present as Fe^{2+}. Error on repeat analysis of standard reference materials was <1% of measured values. *Kα* X-ray lines were monitored for 20–60 s for each element, depending on expected concentrations with the exception of Na *Kα*, which was monitored for only 10 s. Background measurements were performed on either side of each peak position for combined counting times equaling the corresponding peak counting times. Measured peak and background positions were found to be free of interferences within the sample and standard matrices. The analyses were carried out on plagioclase, olivine, pyroxene, amphibole, biotite, Fe–Ti oxides, and glassy groundmass. The analyses obtained in the microprobe correspond to the total sum of oxides >98 wt.% for anhydrous phases and >95 wt.% for hydrous phases. In the cases of the analyses in biotite and Fe–Ti oxides, the analyses with a total >93 wt.% were used since the majority were shown with low values by the microprobe. The cations per formula unit were calculated using the weight percentage obtained by the microprobe and molecular weight of each oxide, taking into account the amount of oxygen present in the chemical formula of each mineral. For Fe–Ti oxides, the total iron content was recalculated by the Carmichael (1967) method to obtain de FeO and Fe_2O_3 contents.

3.2 Whole-Rock Chemistry

The nine samples were analyzed for whole-rock chemistry at Actlabs laboratories (Colombia and Canada). Major elements were analyzed using the ICP-OES (Inductively Coupled Plasma Optical Emission Spectrometry) technique, while trace elements were analyzed using the ICP-MS (Inductively Coupled Plasma Mass Spectrometry) technique. The samples were run for major and selected trace elements on a combination simultaneous/

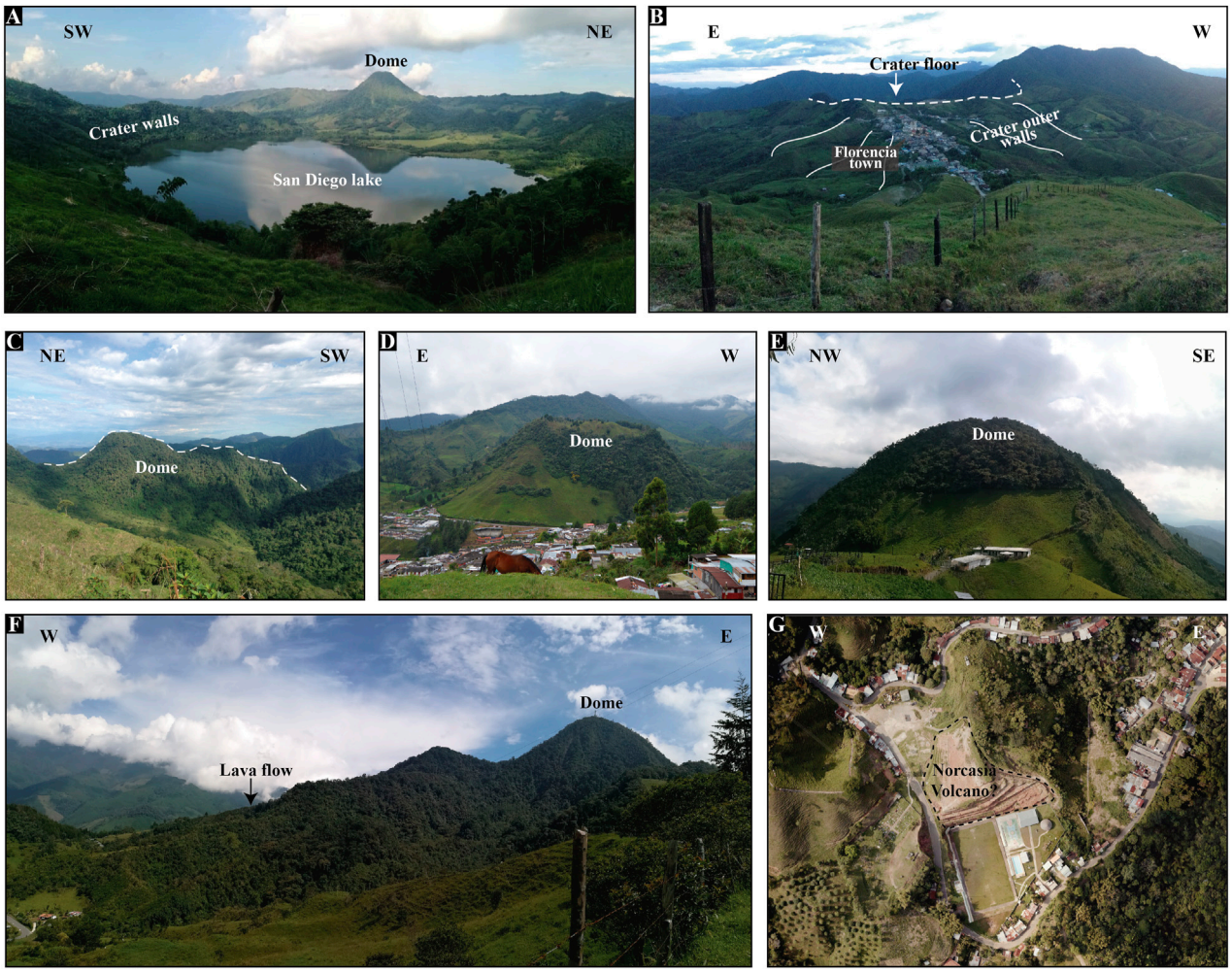

FIGURE 2 | Photographs of the volcanoes of Samaná monogenetic volcanic field **(A)** San Diego maar. The lake is 1 km wide. **(B)** El Escondido tuff cone. **(C)** Pela Huevos dome. **(D)** Piamonte dome. **(E)** Morrón dome. **(F)** Guadalupe dome. Note the lava flow westward. **(G)** Norcasia volcano. It has an undefined volcanic form; orthophoto: Carlos Borrero.

sequential Thermo Jarrell-Ash ENVIRO II ICP for a Varian Vista 735 ICP. Calibration was performed using seven prepared USGS- and CANMET-certified reference materials. For the lithium metaborate/tetraborate fusion—ICP/MS portion of the analysis, the samples were fused, diluted, and analyzed by Perkin Elmer Sciex ELAN 6000, 6100, or 9000 ICP/MS. Loss-on-Ignition (LoI) was calculated from the weighed samples, and iron was reported as total Fe_2O_3. >100x detection limit ±5% for major oxides and >100x detection limit ±100% for minor and trace elements. The sample IIES-V-007 from the Guadalupe volcano yielded a high LoI value (~7 wt.%), and therefore it was not used for major whole-rock and geothermobarometric analysis.

3.3 Geochronology

Three samples from Guadalupe, Piamonte, and Morrón volcanoes were collected for K/Ar geochronology. The samples were crushed and then sieved to separate the 0.5-mm fraction. From these, 20 g of groundmass was extracted by hand picking in order to date the cooling time of the magma. This avoids overestimating ages by mixing the crystals that would introduce older crystallization ages. Freshness of the groundmass was defined not only by looking at the glass using the microscope but also by using the rock samples with low LoI values as indicated by the whole-rock chemistry results. The dating analyses were carried out in ActLabs (Canada) after a further separation of 2 g of fresh groundmass, where the procedure used is described as follows: aliquots of the samples were weighed into an Al container, loaded into the sample system of the extraction unit, and degassed at 100 °C for 2 days to remove the surface gases. Argon was extracted from the sample in a double vacuum furnace at 1,700 °C. The determination of radiogenic argon content was carried out twice on a MI-1201 IG mass spectrometer by the isotope dilution method using ^{38}Ar as a spike, which was introduced to the sample system prior to each extraction.

The extracted gases were cleaned up in a two-step purification system. Then, pure Ar was introduced into a custom-built magnetic sector mass spectrometer (Reynolds type). Two globally accepted standards (P-207 muscovite and 1/65 "Asia" rhyolite matrices) were measured for ^{38}Ar spike calibration. For age calculations, the international values of constants were used as follows: $\lambda K = 0.581 \times 10^{-10}\ y^{-1}$, $\lambda\beta$- = $4.962 \times 10^{-10}\ y^{-1}$, and ^{40}K = 0.01167 (at.%). Calculated errors were *2σ*.

A paleosol located under volcaniclastic products from Norcasia volcano was also selected for ^{14}C dating. The analysis was carried out at the Center Radiochronology Laboratories, Université Laval (Canada) by the AMS (Accelerator Mass Spectrometry) method. The sample was chemically cleaned, burned, and transformed into CO_2, followed by oxidation and reduction to graphite. The graphite produced was pressed into a target for AMS measurement.

4 RESULTS

4.1 Petrography

The studied rocks (**Table 1**) are characterized by their porphyritic texture (30–45 vol.% crystals). The groundmass is glassy (holohyaline) in El Escondido and Morrón volcanoes; glassy with microlites (hypocrystalline) in Pela Huevos, Piamonte, and Norcasia volcanoes; and microcrystalline and cryptocrystalline in Guadalupe and San Diego volcanoes (**Table 1**). Plagioclase is the most abundant mineral phase in five volcanoes (San Diego, El Escondido, Piamonte, Pela Huevos, and Norcasia; **Table 1**), with at least three populations 1) "clean" crystals, 2) coarse sieve texture crystals (**Figure 3A**), and 3) fine or dusty sieve texture crystals (**Figure 3B**); all populations of plagioclase present twins, normal, reverse, and oscillatory zonation. Of the studied volcanoes, San Diego does not display sieve textures of any kind, and Guadalupe only presents fine sieve textures. Amphibole is the most abundant mineral phase in the other two volcanoes (Morrón and Guadalupe), and it is not present in the San Diego volcano (**Table 1**). Amphibole in El Escondido and Piamonte volcanoes is green and strongly pleochroic (**Figure 3C**), whereas in the other volcanoes, it is dark brown and highly oxidized on the whole crystal and/or on the rims (**Figure 3D**). The two types of amphibole do not coexist together. Amphiboles with disequilibrium textures such as oxidation rims (**Figures 3C–E**) and resorption (**Figure 3D**) are observed in Pela Huevos, Morrón, Guadalupe, Norcasia, and Piamonte volcanoes; the latter only exhibit oxidation rims. Biotite was observed only in El Escondido, Morrón, San Diego, and Guadalupe volcanoes. In San Diego (**Figure 3F**), the biotite is reddish brown and highly oxidized on the whole crystals, while in Guadalupe, some of the biotite crystals show oxidation rims (**Figure 3E**). Quartz (**Figure 3F**) is only present in El Escondido and San Diego volcanoes (**Table 1**). Pyroxene (clinopyroxene and orthopyroxene) appear in Pela Huevos and Norcasia volcanoes (**Figure 3G**; **Table 1**), while olivine is present in Pela Huevos and Guadalupe volcanoes (**Table 1**), commonly surrounded by brown amphibole crystals (**Figure 3H**). Accessory minerals such as Fe–Ti oxides (<1 vol.%) appear in all rock samples. Glomerocrysts (**Figure 3G**) of different mineral associations are also observed (**Figure 3G**; **Table 1**).

4.2 Mineral Chemistry

Plagioclase composition in the studied rocks varies from oligoclase to bytownite. San Diego volcano hosts crystals with a low and narrow An range ($An_{26–32}$), compared (**Figure 4A**) with the other volcanoes —El Escondido ($An_{27–57}$), Pela Huevos ($An_{33–73}$), Guadalupe ($An_{30–58}$), Norcasia ($An_{36–68}$), and Piamonte ($An_{42–74}$). Some crystals in El Escondido, Pela Huevos, Norcasia, Piamonte, and Guadalupe volcanoes show oscillatory compositional zonation (**Figure 5A**), and some others in El Escondido and Pela Huevos volcanoes show reverse zonation (**Figure 5B**). Amphiboles are calcic —tschermakite and magnesio-hastingsite— with only magnesio-hornblende crystals in Pela Huevos and Guadalupe volcanoes (**Figure 4B**), without significant differences between both types of amphibole crystals. Normal (i.e., decreasing Mg# toward the rim; **Figure 5C**) and reverse (i.e., increasing Mg# toward the rim; **Figure 5D**) compositional zonation are common in both amphibole crystals. Biotite is magnesiobiotite in both San Diego and Guadalupe (**Figure 4C**). Unfortunately, we did not get accurate measurements of biotite in El Escondido and Morrón volcanoes. Pyroxene from Norcasia volcano corresponds mainly to enstatite ($Wo_{2–3}$, $En_{70–76}$, $Fs_{21–28}$), diopside, and augite ($Wo_{44–45}$, $En_{41–42}$, $Fs_{13–15}$, and $Wo_{42–44}$, $En_{46–47}$, $Fs_{10–11}$, respectively) (**Figure 4D**). Olivine corresponds to $Fo_{82–88}$ in Pela Huevos volcano and $Fo_{81–83}$ in Guadalupe volcano (**Figure 4E**). Fe–Ti oxides (**Figure 4F**) are magnetite (Morrón: $Usp_{6–89}$ $Mag_{94–11}$ and Guadalupe: $Usp_{4–85}$ $Mag_{96–15}$) and ilmenite (Morrón: $Ilm_{78–92}$ $Hem_{22–8}$, and Guadalupe: $Ilm_{61–91}$ $Hem_{39–9}$). **Table 2** shows representative analyses of all mineral phases; all mineral chemistry data can be found in **Supplementary Material S1**.

4.3 Whole-Rock Chemistry

Whole-rock chemistry analysis shows that the rocks from the SMVF range between andesite and dacite (**Figure 6A**), with those from San Diego (SiO_2 ~69 wt.%) and El Escondido (SiO_2 ~66 wt.%) being the most evolved of the group and those from Norcasia, Morrón, and Guadalupe the least evolved (SiO_2 ~60 wt.%). All samples are of a calc-alkaline affinity, with medium potassium content (**Figure 6B**). The studied rocks show similar behavior of the incompatible trace elements, with a slight enrichment in LILE with respect to HFSE (**Figure 6C**). Positive anomalies of Ba, U, K, Pb, Sr, and Nd and negative anomalies of Th, Nb, Ti, and P are observed, with the exception of the San Diego volcano, which lacks a Ti anomaly (**Figure 6C**). Rare earth elements (REE), normalized to chondrite, show a strong LREE enrichment with respect to HREE. Of all the volcanoes, the samples from Morrón and San Diego are the most and least enriched, respectively (**Figure 6D**). Incompatible element ratio diagrams (Nb/Th vs. Nb/Zr and Zr/Y vs. Nb/Th) show similar ratios for all the samples, with only San Diego as an outlier (**Figure 6E**). Binary diagrams of major and trace elements vs. SiO_2 show similar compositions between San Diego and El Escondido volcanoes, between Piamonte and

TABLE 1 | Mineralogical composition and textures present in the rocks of Samaná monogenetic volcanic field.

Volcano	**San Diego**	**El Escondido**	**Piamonte**	**Pela Huevos**	**Pela Huevos**	**Morrón**	**Guadalupe**	**Guadalupe**	**Norcasia**
Sample	**IIES-V-006**	**IIES-V-001**	**IIES-V-008**	**IIES-V-002**	**IIES-V-004**	**IIES-V-130**	**IIES-V-007**	**IIES-V-132**	**IIES-V-009**
Type of sample	**Lithic fragment from the dome**	**Pumice fragment within deposits**	**Lava dome fragment**	**Lava dome fragment within El Escondido deposits**	**Lava dome fragment**	**Lava dome fragment**	**Lava dome fragment**	**Lava dome fragment within deposit**	**Lithic fragment within deposits**
Coordinates	**5°39'31.04"N**	**5°31'19.04"N**	**5°22'28.63"N**	**5°31'19.04"N**	**5°30'47.39"N**	**5°22'47.09"N**	**5°16'18.60"N**	**5°16'14.27"N**	**5°34'20.39"N**
	74°56'33.96"W	**75°2'28.62"W**	**75°9'49.40"W**	**75°2'28.62"W**	**75°2'34.66"W**	**75°6'50.54"W**	**75°8'38.40"W**	**75°7'26.96"W**	**74°53'32.64"W**
Mineral (vol.%)									
Plagioclase	15.3	7.0	20.2	22.0	27.9	14.0	9.7	11.9	27.0
Amphibole	—	2.9	12.5	15.1	15.4	15.2	24.8	20.5	10.5
Biotite	14.2	1.5	—	—	—	0.9	1.2	0.9	—
Quartz	6.0	1.4	—	—	—	—	—	—	—
Pyroxene	—	—	—	1.6	0.8	—	—	—	7.5
Olivine	—	—	—	2.1	0.6	—	0.6	—	—
Groundmass (vol.%)	64.5	44.5	67.3	59.2	55.3	69.9	63.7	66.7	55.0
Vesicles (vol.%)	—	42.7	—	—	—	—	—	—	—
Total	100	100	100	100	100	100	100	100	100
Groundmass textures									
Glassy		✓				✓			
Glassy with microcrysts			✓	✓	✓				✓
Micro and cryptocrystalline	✓						✓	✓	
Glomeroporphyritic textures									
Pl	✓	✓	✓	✓	✓	✓	✓	✓	✓
Amp		✓	✓	✓	✓	✓	✓	✓	✓
Px				✓	✓				✓
Pl and Amp		✓	✓	✓	✓	✓	✓	✓	✓
Amp and Px				✓	✓				✓

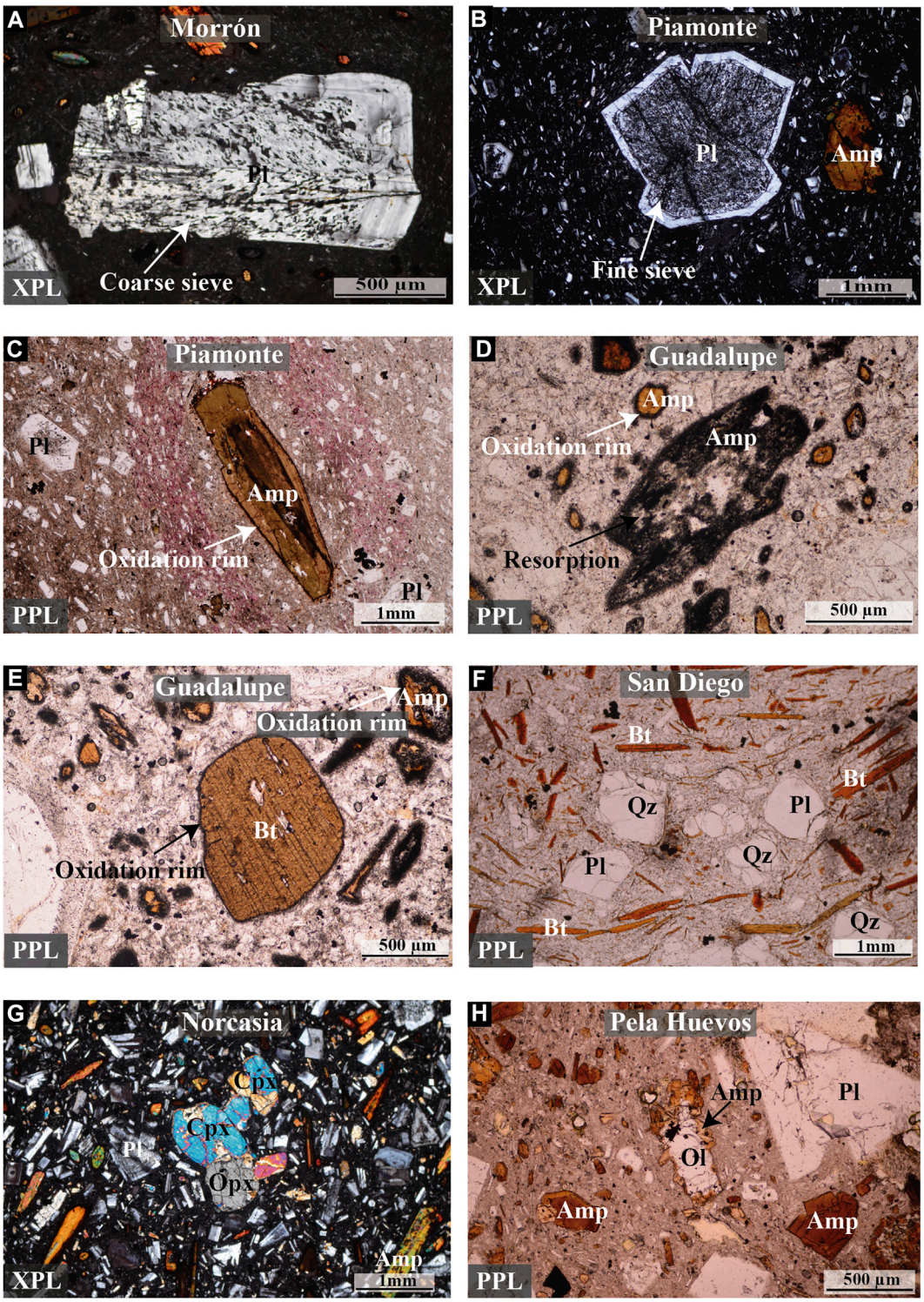

FIGURE 3 | Photomicrographs of petrographic characteristics. **(A)** Coarse sieve texture in plagioclase. **(B)** Fine sieve texture in plagioclase surrounded by a clean rim. **(C)** Green amphibole with an oxidation rim. **(D)** Brown amphibole crystals with oxidation rims and resorption texture. **(E)** Biotite and amphibole crystals with oxidation rims. **(F)** Quartz crystals and biotite with oxidation rims. **(G)** Clinopyroxene and orthopyroxene glomerocryst. **(H)** Olivine surrounded by brown type amphibole.

Pela Huevos volcanoes, and between Morrón, Guadalupe, and Norcasia volcanoes (**Figure 7**). A negative correlation between TiO_2, Al_2O_3, MgO, CaO, Sr, V, and Sc with respect to SiO_2 can be recognized and a positive correlation with K_2O (**Figure 7**). Whole-rock chemistry data from all samples are reported in **Table 3**.

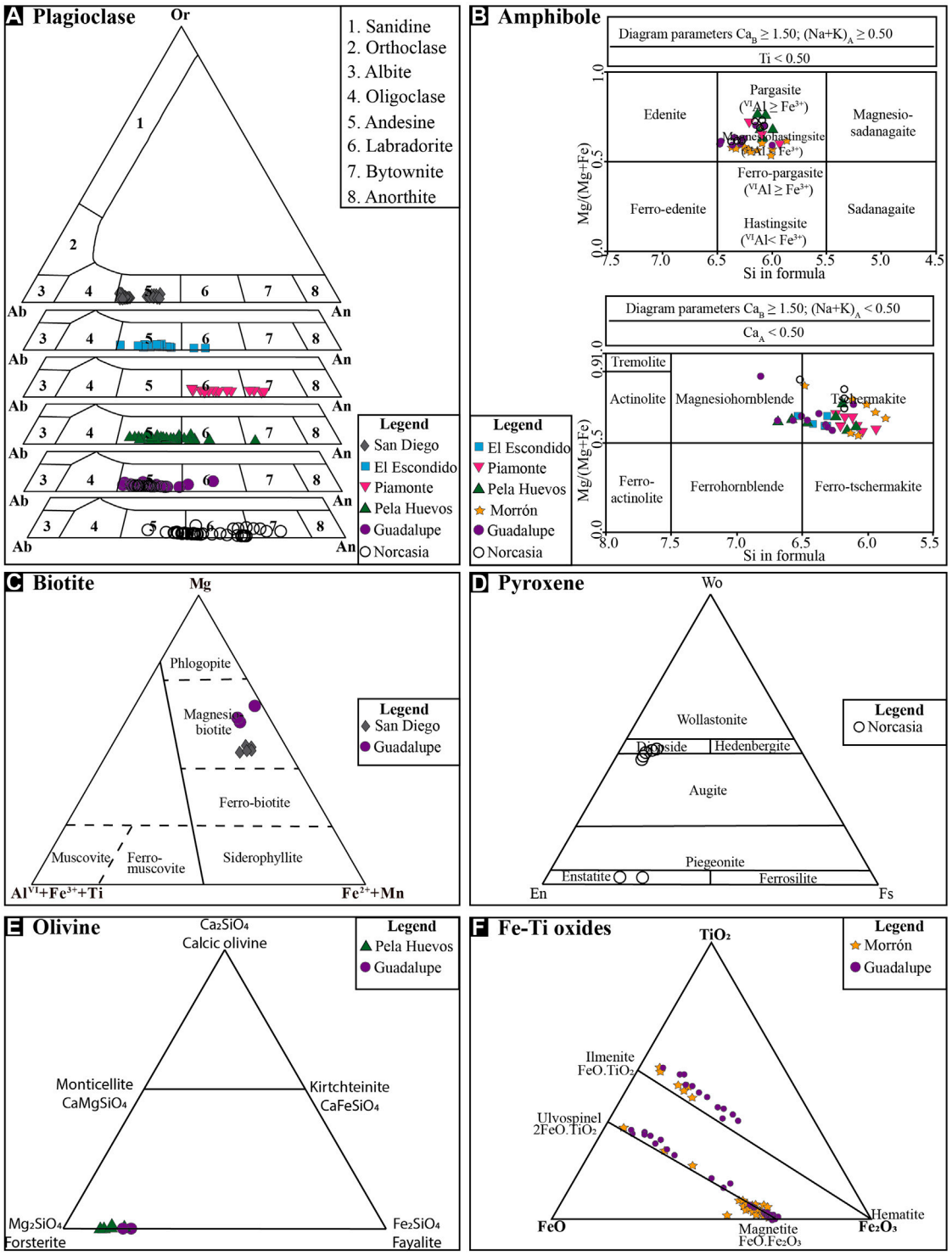

FIGURE 4 | Mineral classification diagrams. **(A)** Plagioclase (Rahman & MacKenzie, 1969). **(B)** Amphibole (Leake et al., 1997). **(C)** Biotite (Foster, 1960). **(D)** Pyroxene (Morimoto, 1989). **(E)** Olivine. **(F)** Fe–Ti oxides (after Parat et al., 2005).

4.4 Geochronology

The K/Ar analysis yields eruptive ages of 0.05 ± 0.04 Ma for the Guadalupe volcano, 0.46 ± 0.04 Ma for the Piamonte volcano, and 1.32 ± 0.06 Ma for the Morrón volcano, while the ^{14}C analysis yielded an age of 16,919 ± 220 years Cal BP for the Norcasia volcano. These ages together with the ages already known for San

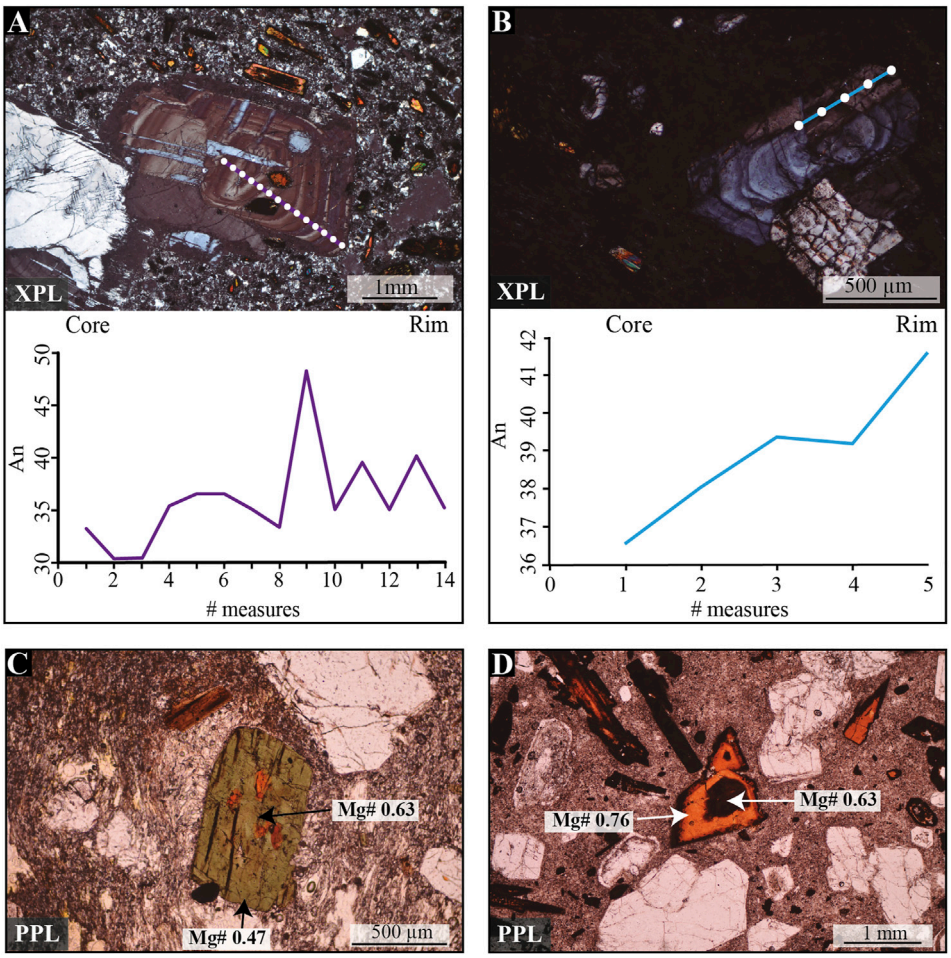

FIGURE 5 | Compositional zonation in plagioclase and amphibole crystals. **(A)** Oscillatory zonation in plagioclase crystal from the Guadalupe volcano (R: rim and C: Core); the white dots represent the measurement points. **(B)** Reverse zonation in the plagioclase crystal from the El Escondido volcano (R: rim, C: Core); the white dots represent the measurement points. **(C)** Normal zonation in the tschermakitic amphibole crystal from El Escondido volcano. **(D)** Reverse zonation in the magnesiohastingsitic amphibole crystal from the Pela Huevos volcano.

Diego (20,056 ± 96 years Cal BP, ^{14}C; Borrero et al., 2017), El Escondido (38,553 ± 596 years Cal BP, ^{14}C; Sánchez-Torres et al., 2019), and Pela Huevos (153,700 ± 38,500 years, ^{40}Ar-^{39}Ar on amphibole; Rueda-Gutierrez, 2019) volcanoes (**Table 4**) indicate that the Samaná field is a long-lived (~1.3 Ma—17 ka) monogenetic volcanic field. In addition, ages indicate that the area is volcanogenic and therefore, the limit previously considered non-volcanogenic due to flat subduction angles begins at ~6°N and not at 5° (c.f. Londoño et al., 2020).

5 DISCUSSION

5.1 Mineral Textures

The wide textural variation identified in the volcanoes forming the SMVF allows us to infer physicochemical processes that the distinct magma batches were subject to, from the source to surface. The existence of both monomineralic and polymineralic glomeroporphyritic texture is indicative of convective movements in the magma (Hogan, 1993; Jeffery et al., 2013), suggesting stagnation zones linked to crystallization, as the magma ascended. This occurred in all magma batches as both glomeroporphyritic texture types were observed in all analyzed rocks (**Table 1**). Changes in the intrinsic parameters of magma (i.e., pressure, temperature and/or water content in the melt) produced disequilibrium between the crystals and the liquid, and therefore features such as zonation, resorption, and oxidation rims were found (c.f. Best, 2003). Reverse zonation in plagioclase crystals from El Escondido and Pela Huevos volcanoes may be associated with crystals that grew in slowly cooled melts or in melts with high concentrations of volatile components (Loomis, 1982). The oscillatory zonation, which is very common in El Escondido, Pela Huevos, Guadalupe, and Norcasia, is associated with kinetic effects and/or convective movements of the magma within the magmatic reservoir (Pearce & Kolisnik, 1990; Berlo et al., 2007; Shcherbakov et al., 2010; Viccaro et al., 2010). Resorption textures (Guadalupe, Pela Huevos, and Morrón volcanoes) and oxidation rims in

TABLE 2 | Representative mineral chemistry analyses from rocks of the Samaná monogenetic volcanic field. Abbreviations: SDV, San Diego volcano; EEV, El Escondido volcano; PV, Piamonte volcano; PHV, Pela Huevos volcano; GV, Guadalupe volcano; NV, Norcasia volcano; MV, Morrón volcano; Pl, plagioclase; Amp, Amphibole; Opx, Orthopyroxene; Cpx, clinopyroxene; Ol, olivine; Bt, biotite; Ilm, ilmenite; Mt, magnetite; and Usp, ulvospinel.

Volcano	**SDV**	**EEV**	**PV**	**PHV**	**GV**	**NV**	**EEV**	**PV**	**PHV**	**MV**	**GV**	**NV**	**NV**	**NV**	**PHV**	**GV**	**SDV**	**GV**	**MV**	**GV**
Mineral	**Pl**	**Pl**	**Pl**	**Pl**	**Pl**	**Pl**	**Amp**	**Amp**	**Amp**	**Amp**	**Amp**	**Amp**	**Opx**	**Cpx**	**Ol**	**Ol**	**Bt**	**Bt**	**Ilm**	**Mt**
Code	**C4pl6**	**C13pl4**	**C3pl2**	**C8Pl3**	**C6Pl18**	**C5Pl2**	**C4b**	**C5a**	**C10b**	**130anf9**	**132anf3**	**C3a**	**C6a**	**C4a**	**C11b**	**C2a**	**C4c**	**C1a**	**Ox30**	**Ox36**
wt.%																				
SiO_2	60.29	54.31	54.16	49.02	60.97	50.27	44.47	41.52	41.88	43.07	45.17	42.09	54.89	50.59	40.8	38.89	35.50	36.53	0.65	0.11
TiO_2							1.29	2.01	1.79	0.98	0.94	2.32	0.14	0.28			2.43	3.14	46.34	28.47
Al_2O_3	23.54	29.02	28.48	31.19	24.15	30.53	11.34	12.61	12.98	12.53	11.75	12.15	1.73	3.69			16.38	14.77	0.31	0.37
FeO_T	0.08	0.23	0.23	0.23	0.12	0.44	14.71	12.81	15.10	16.07	15.10	11.45	14.39	8.01	11.3	16.27	18.87	15.879	43.87	63.73
MnO							0.55	0.17	0.29	0.00	0.00	0.14	0.27	0.25	0.2	0.27	0.29	0.10	1.40	1.15
MgO							12.76	13.15	12.13	11.93	12.27	14.49	27.83	14.53	47.3	43.93	11.98	14.32	2.89	3.39
CaO	5.47	11.73	11.23	15.05	6.23	14.15	10.36	11.35	11.21	11.20	9.86	11.11	1.28	21.13	0.1	0.0				
Na_2O	8.59	4.84	5.47	3.08	7.67	3.53	1.83	2.30	2.20	2.70	3.57	2.54	0.06	0.57			0.82	1.03		
K_2O	0.29	0.12	0.13	0.08	0.41	0.13	0.36	0.54	0.40	0.63	0.60	0.51					8.37	8.26		
TOT	98.23	100.23	99.72	98.68	99.52	99.06	97.70	96.48	97.99	99.11	99.26	96.85	100.58	99.07	99.8	99.44	94.61	93.90	95.40	97.26
Fe_2O_3**																			8.87	14.20
FeO**																			35.89	50.95
Cations per formula unit																				
Si	2.73	2.45	2.46	2.27	2.72	2.32	*	*	*	*	*	*	1.96	1.90	1.01	0.99	5.44	5.55	0.02	0.00
Ti							*	*	*	*	*	*	0.00	0.01			0.28	0.36	0.92	0.83
Al	1.26	1.54	1.52	1.70	1.27	1.66	*	*	*	*	*	*	0.07	0.16			2.96	2.65	0.01	0.02
Fe^{+3}	0.00	0.00	0.00	0.00	0.00	0.00	*	*	*	*	*	*	0.01	0.07	0.00	0.00	0.00	0.00	0.00	0.00
Fe^{+2}	0.00	0.01	0.01	0.01	0.00	0.02	*	*	*	*	*	*	0.42	0.18	0.23	0.35	2.42	2.01	0.97	2.07
Mn							*	*	*	*	*	*	0.01	0.01	0.00	0.01	0.04	0.01	0.03	0.04
Mg							*	*	*	*	*	*	1.48	0.81	1.74	1.67	2.74	3.24	0.11	0.20
Ca	0.27	0.57	0.61	0.75	0.30	0.70	*	*	*	*	*	*	0.05	0.85	0.00	0.00				
Na	0.75	0.42	0.40	0.28	0.66	0.32	*	*	*	*	*	*	0.00	0.04			0.24	0.30		
K	0.02	0.01	0.01	0.00	0.02	0.01	*	*	*	*	*	*					1.63	1.60		
Sum	5.02	5.00	5.03	5.02	4.98	5.02							4.00	4.03	2.99	3.01	15.7	15.7	2.06	3.16
Mg#													77.5	76.4	88.2	82.8				
X_{An}	25.6	56.8	52.8	72.6	30.3	68.4														
$X_{Ilm/Usp}$																			90.6	78.6

*Mg#, (Mg//Mg + Fe) x100; An, (Ca/ (Ca + Na + K) x100; Ilm and Usp, calculated after Stormer (1983) as outlined in Lepage (2003). **Oxides Fe separation after Carmichael (1967). Cations per formula unit calculated based on 8, 6, 4, and 22 oxygens for plagioclase, pyroxene, olivine, and biotite, respectively. For amphibole, formula based on 13 cations was used (eCNK). For ilmenite and magnetite, three and four oxygens, respectively, were used for the calculations. *See* ***Supplementary Material S1****.*

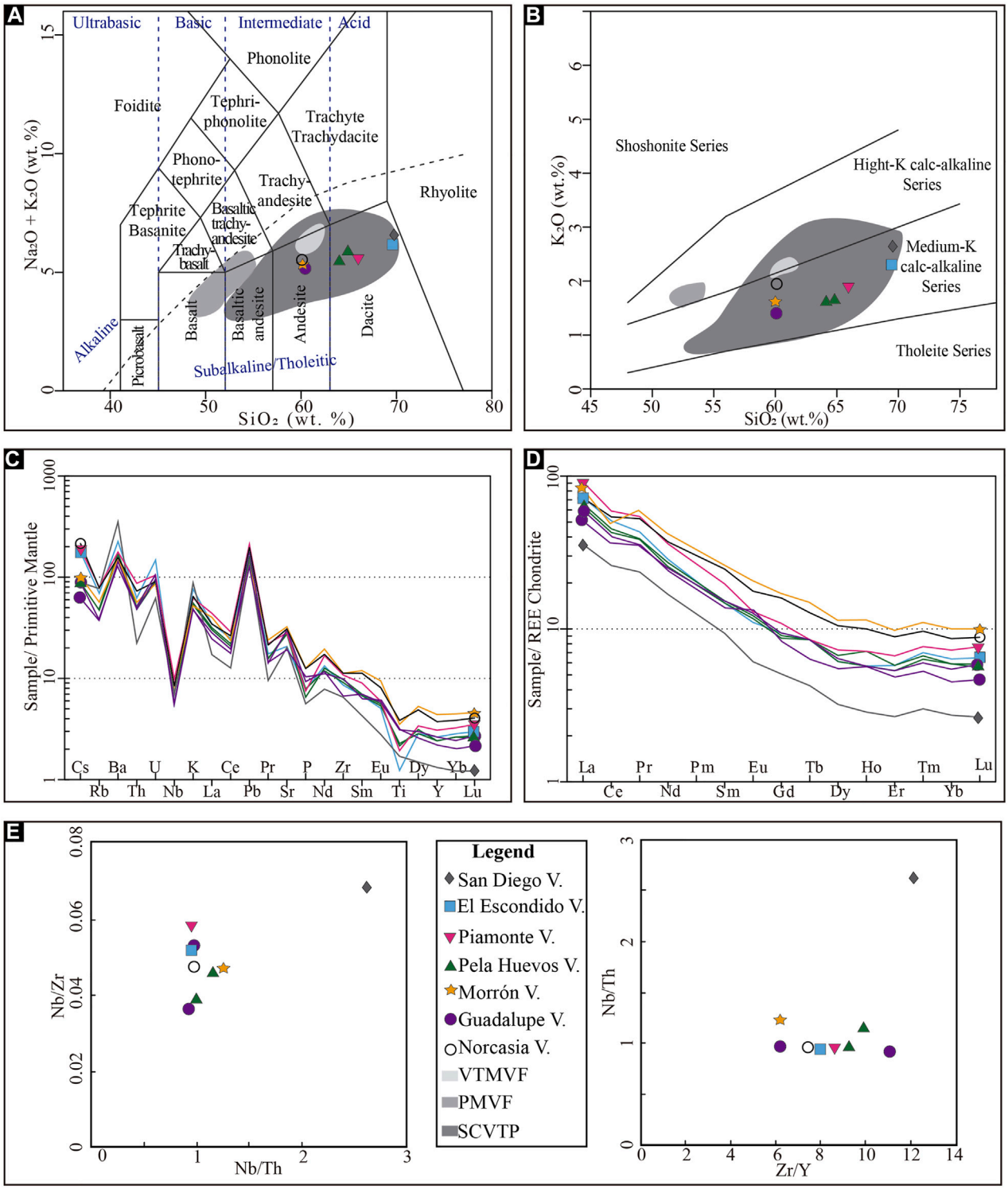

FIGURE 6 | Whole-rock geochemistry diagrams. **(A)** TAS (Total Alkali Silica) diagram (Le Bast et al., 1986). **(B)** Magma type classification diagram (Peccerillo & Taylor, 1976). **(C)** Multielement diagram normalized to primitive mantle (Sun & McDonough, 1989). **(D)** REE multielement diagram normalized to chondrite (Nakamura, 1974). **(E)** Incompatible element ratio diagram. SCVTP, San Diego—Cerro Machín Volcano-Tectonic Province (Cavell, 2020; and references therein); PMVF, Pijaos monogenetic volcanic field (Velandia et al., 2021); and VTMVF, Villamaría–Termales monogenetic volcanic field (Salazar-Muñoz et al., 2021).

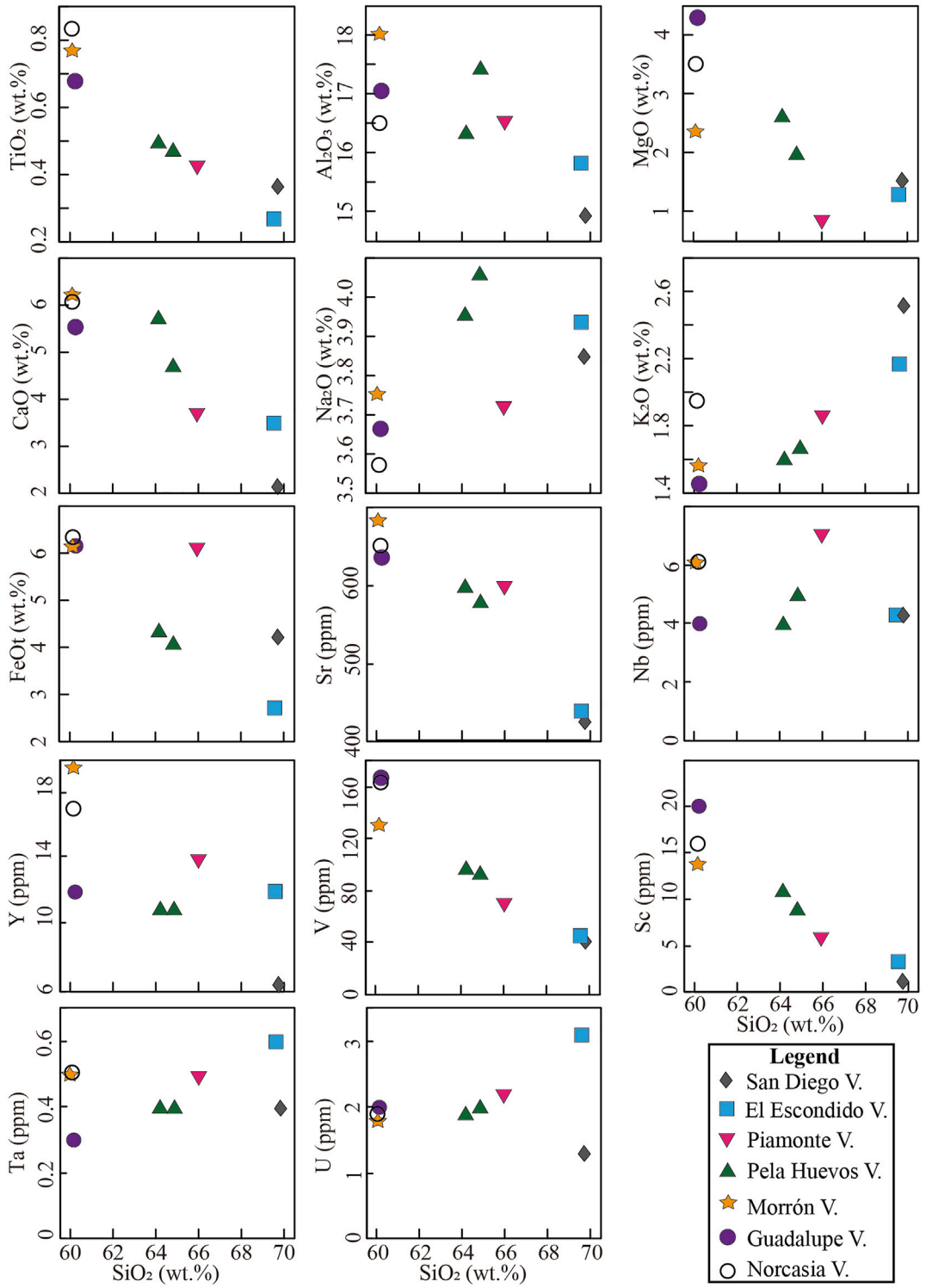

FIGURE 7 | SiO_2 vs. major and trace elements diagrams. Note the affinity shared by the volcanoes based on the silica content.

amphibole (Piamonte, Pela Huevos, Morrón, Guadalupe, and Norcasia volcanoes) and biotite crystals (Guadalupe and Morrón volcanoes) probably occurred due to the loss of water in the melt caused by decompression during magma ascent (Gill, 1981; Rutherford & Hill, 1993; Ridolfi et al., 2008) and/or the dehydrogenation of the melt (Feeley & Sharp, 1996). Coarse sieve texture in plagioclase crystals from El Escondido, Piamonte, Pela Huevos, Morrón, and Norcasia volcanoes is

TABLE 3 | Whole-rock chemical data of investigated rocks of the Samaná monogenetic volcanic field.

Sample	IIES-V-006 (San Diego volcano)	IIES-V-001 (El Escondido volcano)	IIES-V-008 (Piamonte volcano)	IIES-V-002 (Pela Huevos volcano)	IIES-V-004 (Pela Huevos volcano)	IIES-V-130 (Morrón volcano)	IIES-V-132 (Guadalupe volcano)	IIES-V-007 (Guadalupe volcano)	IIES-V-009 (Norcasia volcano)
Wt.									
SiO_2	68.50	66.47	64.60	63.62	63.89	58.88	59.46	56.94	59.58
Al_2O_3	14.66	15.11	16.19	16.16	17.15	17.67	16.84	17.38	16.35
Fe_2O_3	4.61	2.88	6.61	4.81	4.48	6.67	6.75	6.09	6.98
FeOt	4.15	2.59	5.95	4.33	4.03	6.00	6.07	5.48	6.28
MnO	0.10	0.13	0.11	0.11	0.12	0.14	0.12	0.10	0.12
MgO	1.50	1.24	0.80	2.58	1.97	2.33	4.24	3.77	3.47
CaO	1.99	3.34	3.59	5.70	4.68	6.08	5.44	3.91	6.03
Na_2O	3.78	3.76	3.64	3.92	4.00	3.68	3.62	2.54	3.54
K_2O	2.60	2.20	1.83	1.60	1.65	1.54	1.44	1.34	1.93
TiO_2	0.36	0.26	0.41	0.49	0.46	0.75	0.66	0.63	0.83
P_2O_5	0.12	0.16	0.16	0.17	0.14	0.27	0.20	0.21	0.27
LOI	0.66	3.13	1.64	1.22	1.18	2.21	1.88	7.63	1.23
Total	98.87	98.67	99.58	100.40	99.72	100.20	100.70	100.50	100.30
ppm									
Sc	4.00	6.00	6.00	11.00	9.00	14.00	20.00	17.00	16.00
Be	2.00	2.00	2.00	1.00	1.00	2.00	2.00	1.00	1.00
V	39.00	44.00	70.00	96.00	93.00	132.00	163.00	147.00	167.00
Cr	—	—	200.00	80.00	30.00	40.00	110.00	90.00	90.00
Co	6.00	5.00	5.00	10.00	8.00	12.00	18.00	16.00	18.00
Zn	100.00	50.00	100.00	50.00	50.00	100.00	80.00	90.00	120.00
Rb	49.00	44.00	51.00	30.00	31.00	36.00	24.00	24.00	50.00
Sr	426.00	437.00	595.00	599.00	579.00	683.00	635.00	406.00	650.00
Y	6.00	12.00	14.00	11.00	11.00	20.00	12.00	10.00	17.00
Zr	73.00	96.00	121.00	102.00	109.00	126.00	75.00	111.00	126.00
Nb	5.00	5.00	7.00	4.00	5.00	6.00	4.00	4.00	6.00
Cs	0.70	1.40	1.50	0.70	—	0.80	0.70	0.50	1.70
Ba	2461.0	1572.0	1237.0	1103.0	1211.0	1055.0	1001.0	899.0	1 092.0
La	11.80	23.90	30.30	20.80	21.80	27.60	16.90	19.50	23.70
Ce	22.50	44.10	51.10	37.00	39.10	44.00	31.40	34.70	46.80
Pr	2.64	4.83	6.09	4.31	4.36	6.62	3.92	3.98	5.90
Nd	10.60	18.00	22.70	16.10	17.10	26.40	15.80	15.10	23.40
Sm	2.00	3.00	4.00	3.00	3.00	5.00	3.00	2.80	3.00
Eu	0.47	0.85	1.00	0.90	0.94	1.59	0.98	1.08	1.36
Gd	1.40	2.60	3.00	2.40	2.50	4.70	2.60	2.30	4.40
Tb	0.20	0.40	0.40	0.40	0.40	0.70	0.40	0.30	0.60
Dy	1.10	2.10	2.50	2.10	2.30	3.90	2.20	1.90	3.60
Ho	0.20	0.40	0.50	0.40	0.50	0.80	0.40	0.40	0.70
Er	0.60	1.30	1.50	1.20	1.30	2.20	1.20	1.10	2.00
Tm	0.09	0.21	0.23	0.19	0.20	0.33	0.18	0.16	0.29
Yb	0.60	1.40	1.60	1.30	1.30	2.20	1.20	1.00	1.90
Lu	0.09	0.22	026	0.19	0.20	0.34	0.20	0.16	0.30
Hf	2.80	2.40	3.50	2.60	2.70	3.60	2.20	2.80	3.80
Ta	0.40	0.60	0.50	0.40	0.40	0.50	0.30	0.30	0.50
Ti	0.20	0.10	0.40	—	—	0.30	—	—	0.30
Pb	9.00	11.00	15.00	11.00	9.00	9.00	13.00	9.00	14.00
Th	1.90	5.60	7.40	4.10	4.60	4.80	4.10	4.30	6.20
U	1.30	3.10	2.20	1.90	2.00	1.80	2.00	2.20	1.90

FeO, FeOt = Fe_2O_3 × 0.8998.

associated with disequilibrium due to decompression and fast ascent rates that produced dissolution in the crystals (Nelson & Montana, 1992; Monfaredi et al., 2009; Viccaro et al., 2010; Viccaro et al., 2012), while fine sieve texture in all volcanoes (but San Diego) is formed by partial melting of the crystal due to the reaction linked to the influx of magma (i.e., magma recharge or mixing); therefore, the clean rims that surround the dusty zone are interpreted as being formed by overgrowth at a post-mixing stage (Tsuchiyama, 1985; Viccaro et al., 2010; Viccaro et al., 2012).

Taking the aforementioned characteristics, we propose that, at the SMVF, the magma that fed the volcanoes was affected by sudden changes in pressure, temperature, melt water content, and convective movements. However, the San Diego volcano is the

TABLE 4 | Ages of volcanic products in the Samaná monogenetic volcanic field.

Volcano	Age		Method	Reference
	Uncalibrated	Calibrated		
Morrón	—	1.32 ± 0.06 Ma	K/Ar on whole rock	This work
Piamonte	—	0.46 ± 0.04 Ma	K/Ar on whole rock	This work
Pela Huevos	—	153,700 ± 38,500 years	Ar-Ar on amphibole	Rueda-Gutiérrez (2019)
Guadalupe	—	0.05 ± 0.04 Ma	K/Ar on whole rock	This work
El Escondido	34,060 ± 240 years BP	38,553 ± 596 years Cal BP[a]	^{14}C on charcoal	Sánchez-Torres et al. (2019)
	33,230 ± 220 years BP	37,484 ± 798 years Cal BP[a]	^{14}C on charcoal	Sánchez-Torres et al. (2019)
San Diego	16,624 ± 48 years BP	20,056 ± 93 years Cal BP[a]	^{14}C on paleosol	Borrero et al. (2017)
Norcasia	13,960 ± 220 years BP	16,919 ± 629 years Cal BP[a]	^{14}C on paleosol	This work

[a]*Calibrated age using the program Oxcall 4.3. See website https://c14.arch.ox.ac.uk/oxcal.html#program. Probability used to calibrate: 95.4%. Calibration curve used, IntCall13.*

most stable system in relation to the other volcanoes due to little evidence of disequilibrium of its mineral phases. In summary, the textural analysis of SMVF volcanoes suggests that the magmas had periods of stagnation before eruption. During these periods, convective movement of the magma, followed by decrease of pressure, gave rise to different degrees of resorption and disequilibrium processes in the different mineral phases. Later, the ascent of magma with degassing produced destabilization and oxidation of the previously formed crystals; this process was continuous to shallow levels.

5.2 Geothermobarometry

Two types of geothermobarometers were applied to obtain crystallization conditions of the main mineral phases identified in the volcanic products from the SMVF 1) based on mineral–liquid chemical equilibrium, which involved olivine, clinopyroxene, orthopyroxene, and plagioclase mineral phases; 2) based on mineral composition, which involved amphibole and Fe–Ti oxides. For the mineral–liquid method, the composition of the liquid was assumed to be the composition of the whole rock for the olivine and pyroxene phases, while for the plagioclase, the composition of the liquid was assumed to be the glass composition based on the partition coefficient (K_D).

Olivine crystals were not found in equilibrium ($K_{D\ Fe\text{-}Mg}$: 0.27 ± 0.03), which in turn suggests that these crystals correspond to antecrysts or xenocrysts (c.f. Jerram and Martin, 2008; Zellmer, 2021). For clinopyroxene ($K_{D\ Fe\text{-}Mg}$: 0.28 ± 0.08) and orthopyroxene ($K_{D\ Fe\text{-}Mg}$: 0.29 ± 0.06) in equilibrium, the geothermobarometers applied were equations 32d and 32c (clinopyroxene) and 28a and 29b (orthopyroxene) of Putirka (2008). Three out of four clinopyroxene crystal analyses and one out of two orthopyroxene crystal analyses met the equilibrium test. For plagioclase, equations 24a, 25a, and 25b of Putirka (2008) were applied to 212 out of 232 crystal analyses, which were the ones that met the equilibrium test, based on a proxy of ~70 wt.% of SiO_2 liquid and a K_D (An-Ab) of 0.10 ± 0.05 for T <1,050°C. This liquid composition coincides with the glass composition of the Norcasia volcano and therefore was used as the proxy for all volcanoes. In addition, the plagioclase geothermobarometer requires input parameters such as pressure and H_2O; the former was estimated from the clinopyroxene crystallization (0.7 GPa) (c.f. Putirka, 2008) and the latter defined as 3.2 wt.% from the glass composition results. All the plagioclase analyses were applied exclusively to "clean" crystals, with the exception of the Guadalupe volcano, where valid microprobe data (i.e., the total sum of major oxides >98 wt.%) were obtained for crystals with sieve texture only. The results after applying these mineral–liquid chemical geothermobarometers indicate that clinopyroxene crystallized at 1,194–1,165°C and 0.9–0.7 GPa, orthopyroxene crystallized at 1,148°C and 0.6 GPa, and plagioclase crystallized at 943–891°C, 0.8–0.1 GPa, and 4.9–2.9 wt.% H_2O (**Table 5**; **Supplementary Material S2**). The range of the calculated temperatures is narrow and similar between volcanoes, whereas the pressure shows relatively wider ranges but still relative similar among the volcanoes (**Figure 8**). Perhaps the only exception is the pressure range for the plagioclase phase of the San Diego volcano, which is

TABLE 5 | Estimated temperature, pressure, and depth crystallization values of the mineral phases that were identified at the Samaná monogenetic volcanic field.

Geothermobarometer	T (°C)	P (GPa)	Depth (km)
Clinopyroxene Putirka (2008)			
Norcasia volcano	1194–1165	0.88–0.75	33–28
Orthopyroxene Putirka (2008)			
Norcasia volcano	1148	0.56	21
Plagioclase Putirka (2008)			
San Diego volcano	898–891	0.82–0.60	31–23
El Escondido volcano	926–893	0.79–0.17	30–6
Piamonte volcano	928–925	0.17–0.14	6–5
Pela Huevos volcano	926–900	0.59–0.16	23–6
Guadalupe volcano	943–900	0.58–0.31	22–12
Norcasia volcano	929–909	0.51–0.17	19–6
Amphibole Ridolfi & Renzulli (2012)			
El Escondido volcano	932–907	0.41–0.28	15–11
Piamonte volcano	956–898	0.68–0.37	26–14
Pela Huevos volcano	987–868	0.83–0.24	31–9
Morrón volcano	972–899	0.81–0.37	31–14
Guadalupe volcano	934–810	0.40–0.19	15–7
Norcasia volcano	970–862	0.41–0.19	15–8
Fe–Ti Oxides Andersen & Lindsley (1985)			
Morrón volcano	828–745	—	—
Guadalupe volcano	871–687	—	—

Clinopyroxene: T, Eq. 32d; P, Eq. 32c; SEE_T = ±87°C; SEE_P = ±0.5 GPa. Orthopyroxene: T, Eq. 28a; P, Eq. 29b; SEE_T = ±28°C; SEE_P = ±0.21 GPa. Plagioclase: T, Eq. 24a; P, Eq. 25a; SEE_T = ±36°C; SEE_P = ±0.40 GPa. Amphibole: T, Eq. 2; P, Eq. 1a; SEE_T = ±23.5°C; SEE_P = ±11.5%. SEE_T, and SEE_P dictate the standard error of estimate of temperature and pressure for each mineral, respectively.

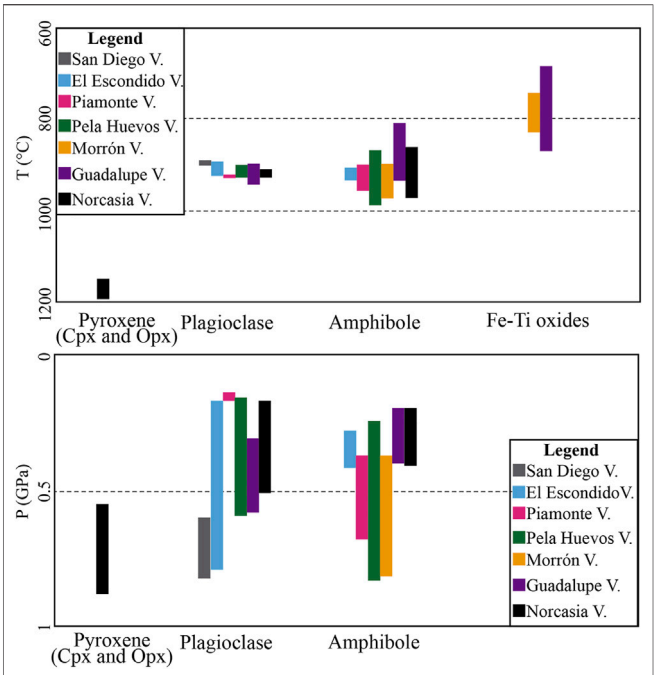

FIGURE 8 | Temperature and pressure ranges of different mineral phases in each volcano as indicated by geothermobarometric results.

noticeably higher (>0.5 GPa) than the other volcanoes. All data obtained including K_D, T (°C), P (GPa), H_2O (wt.%), and log fO_2 are included in **Supplementary Material S2** and summarized in **Table 5**.

A geothermobarometer based solely on the composition of amphibole was evaluated following Ridolfi et al. (2010) for fO_2 and Ridolfi & Renzulli (2012) for T, P, and H_2O melt. Thus, 51 analyses were assessed yielding crystallization conditions of 987–810°C and 0.8–0.2 GPa (**Figures 8**, **9A**). H_2O and fO_2 were also obtained, which yielded values of 12.2–4.3 wt.% H_2O (**Figure 9B**) and −8.6 to −11.5 log fO_2, respectively,(**Figure 9C**). Data for each volcano are discriminated in **Table 5**. The composition of Fe–Ti oxides also allowed us to determine temperature and fO_2, following the geothermobarometer of Andersen & Lindsley (1985) through the ILMAT Excel worksheet (Lepage, 2003) based on the equilibrium between the coexistence of ilmenite and magnetite phases proposed by Bacon & Hirschman (1988). Using the pair of phases that met the equilibrium test, the results indicated crystallization conditions of 871–687°C and −11.9 to −15.8 log fO_2 (**Figure 9C**) (**Table 5**; **Supplementary Material S2**).

The depths at which the different mineral phases crystallized (**Table 5**) were estimated by using the results of the pressure calculations, following White (2013): density × gravity = pressure/depth, and assuming a density of 2.7 g/cm^3 (c.f. Lucassen et al., 2001). Based on this, we estimate that diopside and augite pyroxene crystallized between 33 and 28 km and enstatite pyroxene at 21 km. Plagioclase crystallization occurred between 31 and 5 km. For amphiboles, magnesio-hastingsite crystallized between 31 and 9 km, tschermakite crystallized between 31 and 7 km, and magnesio-hornblende crystallized at 9 km. The **Supplementary Material S2** shows discriminated data for each geothermobarometer.

5.3 Magmatic Evolution

The compositional characteristics of the SMVF (i.e., calc-alkaline affinity, behavior of trace and REE elements) are typical of magmas subduction-related. The enrichment of K, U, and Ba and the negative anomalies of Nb, Ta, and Ti (**Figure 6C**) are typical of volcanic arc rocks and represent processes of fractionation of Fe–Ti oxides and crustal contamination and influence of subduction fluids in the partial fusion of the mantle wedge (Pearce, 1983; Rollinson, 1993; Best, 2003; White, 2013). Incompatible element ratio diagrams (**Figure 6E**) indicate that the volcanoes of the SMVF are likely fed by the same magmatic source, with the exception of the San Diego volcano, whose source chemical characteristics are slightly different.

5.3.1 Fractional Crystallization

Fractional crystallization is a dominant process of magma evolution in arc magmas, which is commonly evidenced by trends observed for major and trace elements (**Figure 7**), including the ratio of highly incompatible ones (**Figures 10A,B**) with respect to SiO_2 (Rollinson, 1993; Davidson et al., 1988). Our results indicate that fractional crystallization is, indeed, a major process in the evolution history of the magmas that formed the SMVF volcanoes; El Escondido volcano shows the highest degree of magma fractionation, and Norcasia, Morrón, and Guadalupe volcanoes exhibit the least fractionated magmas. The Piamonte and Pela Huevos volcanoes represent intermediate degrees of fractional crystallization. Plagioclase fractionation is evidenced by the negative correlation of CaO, Al_2O_3, and Sr, vs. SiO_2 (**Figure 7**) and the CaO/Al_2O_3 ratio (**Figure 10C**). The behavior of Sr is related to the increasing compatibility of this element in sodium plagioclase (rather than in calcium plagioclase; c.f. Davidson et al., 1988; Blundy & Wood, 1991). The lack of significant Eu negative anomalies (**Figure 10F**) supports this fractionation (i.e., Na plagioclase) as Eu plays a role at low oxygen fugacities linked to significant depths (Rollinson, 1993). Amphibole fractionation is evidenced by the enrichment of LREE on HREE (**Figure 6D**) (c.f. Pearce & Norry, 1979; Davidson et al., 1988; Rollinson, 1993) and the negative correlation of Sc, V, and Sm/Nd vs. SiO_2 (**Figures 6**, **10D**) and positive correlation of Yb/Dy vs. SiO_2 (**Figure 10E**). For the pyroxene phase, fractionation is evidenced more clearly in the Norcasia and Pela Huevos volcanoes by the negative correlation of the SiO_2 vs. the CaO/Al_2O_3 ratio (**Figure 10C**) and Sc (**Figure 7**), with Sc mainly related to clinopyroxene (c.f. Green, 1980; Wilkinson and Taylor, 1981; Romick et al., 1992; Williams et al., 2009). Fractionation of Fe–Ti oxides is evidenced by the negative anomalies of Nb, Ta, and Ti (**Figure 6C**), which is in turn consistent with the moderate and highly oxidized environments evidenced for the magmas (**Figure 9C**). As a whole, the linear trends observed in the Harker diagrams that illustrate the composition of the volcanoes of the SMVF (**Figure 7**) and the patterns observed

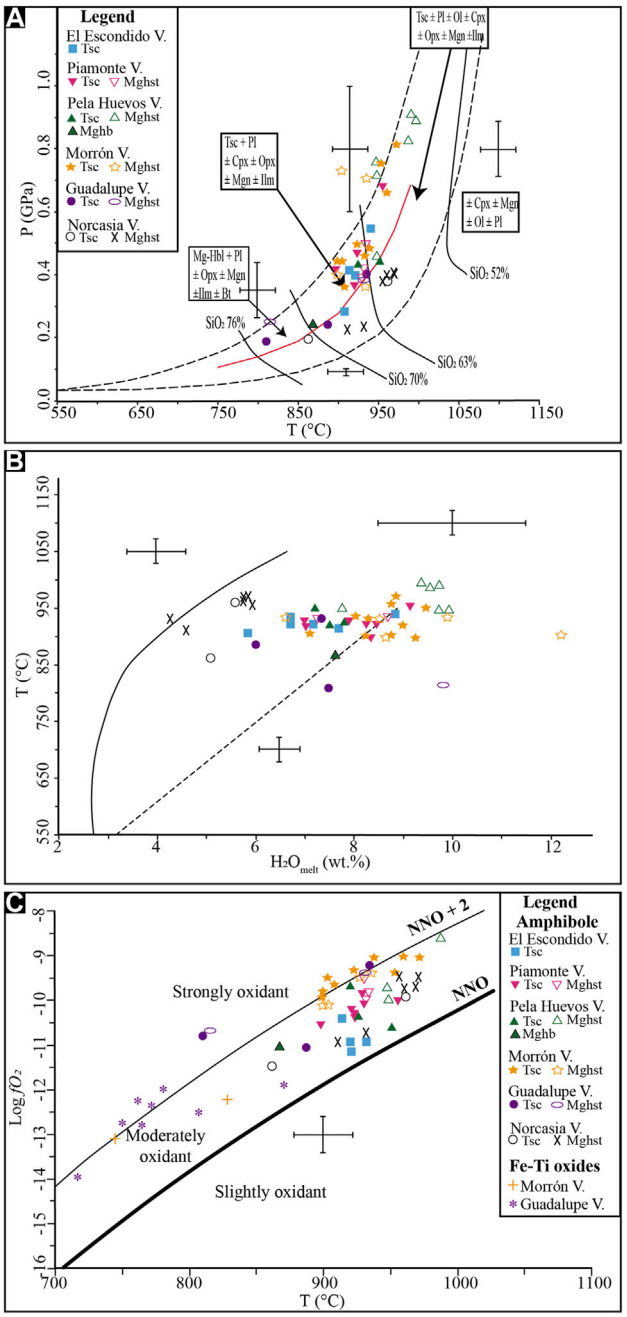

FIGURE 9 | Crystallization conditions based on amphibole geothermobarometry after Ridolfi et al. (2010) and Ridolfi & Renzulli (2012). **(A)** T vs. P diagram, isopleths show the anhydrous SiO_2 (wt.%) content of the melt and P–T stability limits of phases in the boxes, and the black dashed lines represent the maximum thermal stability, and the red line divides consistent experimental product with different crystallinity (35–50 wt.% at lower T and 12–35 wt.% at higher T) (Ridolfi et al., 2010). **(B)** H_2O vs. T melt diagram; the black line represents the maximum thermal stability and black dash line represents the lower limit of amphiboles (Ridolfi et al., 2010). **(C)** T vs. log fO_2 diagram, the curves represent the nickel–nickel oxide (NNO) buffer and NNO+2 (Ridolfi et al., 2010); Fe–Ti oxides (Andersen & Lindsley, 1985) are included in this diagram to observe their crystallization conditions with respect to amphibole. Error bars represent the expected uncertainty in T (± 23.5°C), P (± 11.5%), H_2O melt (15%), and log fO_2 (± 0.4 log units). Abbreviations: (Tsc), tshermakite; (Mgsht), magnesio-hastingsite; and (Mghb), magnesio-hornblende.

(*Continued*)

in approximately constant ratio of similar elements such as Nb/Th and Nb/La with respect to SiO_2 (**Figures 10A,B**) also illustrate fractionation as important in the evolution of the magmas that formed the SMVF volcanoes. This is consistent with recent studies in the region (Cavell, 2020), in which the compositional variations of the Northern Volcanic Province of the Andes (or the San Diego—Cerro Machin Volcano-Tectonic Province) are explained by different degrees of fractional crystallization and the type of fractionating mineral phases.

5.3.2 Crustal Assimilation

Assimilation is a process that can modify the composition of magmas during their rise and/or stagnation in the crust (Best, 2003; Groove & Till, 2015). Its occurrence can be examined by the presence of xenocrysts and/or xenoliths and by comparison with the composition of the basement and variations in the ratio of incompatible elements (Rollinson, 1993). It could be argued that the olivine crystals that did not meet the equilibrium test are xenocrysts and therefore record the process of crustal assimilation. However, the basement rocks in the area do not host this mineral phase and, therefore, an antecryst origin for the olivine seems more plausible (c.f. Jerram & Martin, 2008; Zellmer, 2021). Furthermore, by comparing the variation of incompatible element ratios with respect to SiO_2 (**Figures 10A,B**) for products of the SMVF and the basement rocks of the Cajamarca Complex (the major possible source of crustal contamination), it can be assessed that any contribution of the Cajamarca Complex is negligible. The exception appears in the San Diego volcano, in which the outlier composition could perhaps indicate some degree of assimilation or a different degree of partial melting (**Figures 10A,B**).

5.3.3 Magma Mixing

Magma mixing can occur en route to the surface and/or within a magmatic reservoir, and it is usually explained by processes of magma recharge (Sen, 2014; Groove & Till, 2015). Textural characteristics in the studied rocks, such as the coexistence of crystals in equilibrium and disequilibrium, are interpreted as results of the interaction between two or more melts (c.f. Best, 2003; Varol et al., 2008; Varol et al., 2014). Therefore, the presence of zoned and non-zoned amphiboles within the same sample (as occurs in El Escondido, Piamonte, Pela Huevos, Guadalupe, Norcasia, and Morrón volcanoes) evidence disequilibrium linked to different magma compositions. Equally, disequilibrium textures such as sieve (in El Escondido, Piamonte, Pela Huevos, Guadalupe, Norcasia, and Morrón volcanoes), crystal resorption (in Pela Huevos, Guadalupe, Norcasia, and Morrón volcanoes), and oxidation rims (in Piamonte, Pela Huevos, Guadalupe, Norcasia, and Morrón volcano) vs. in-equilibrium crystals in the same rock could also evidence this process. The possible antecryst origin of the olivine crystals in Guadalupe and Norcasia volcanoes is also

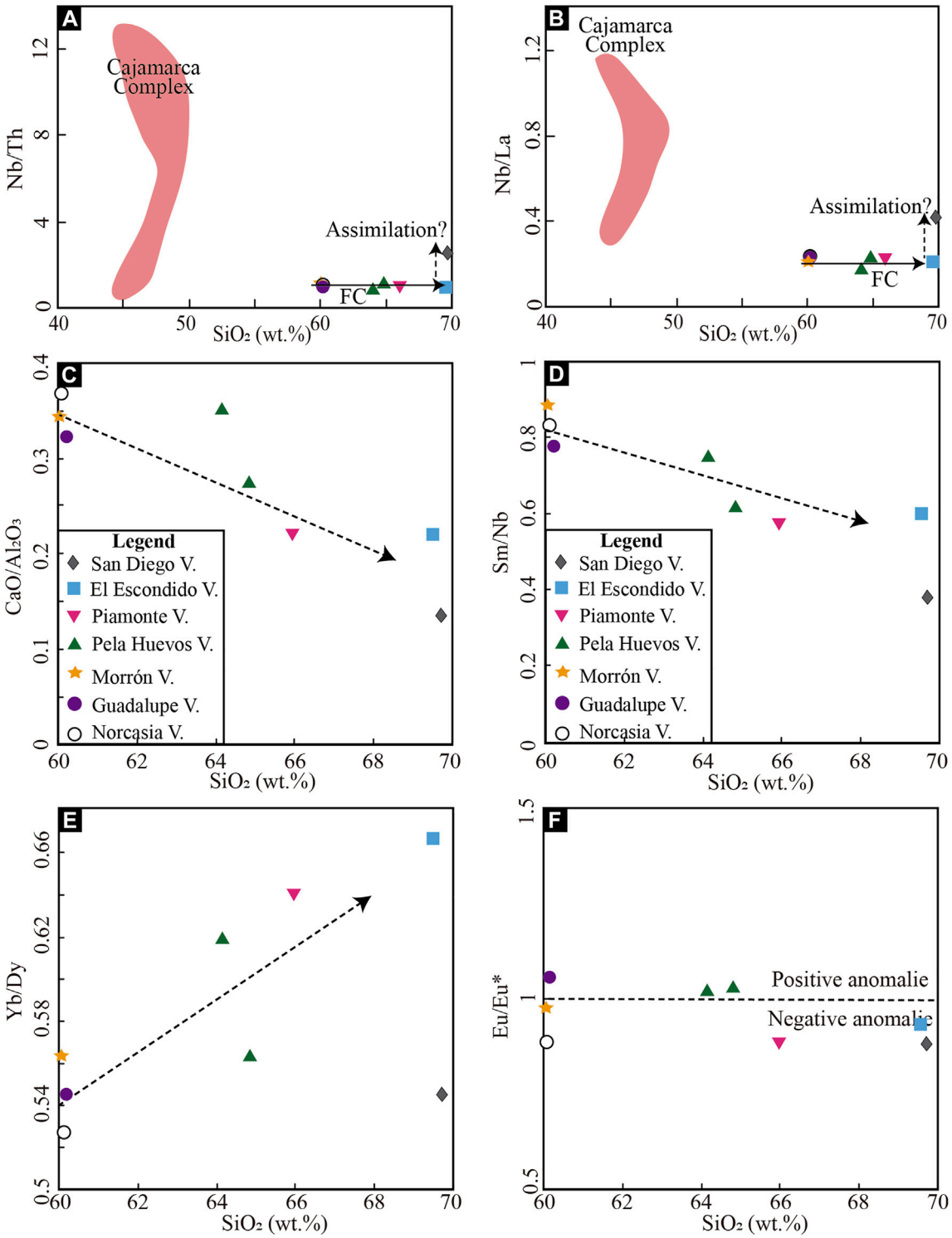

FIGURE 10 | Petrogenetic evolution based on SiO_2 and incompatible trace elements. **(A,B)** Diagrams of SiO_2 vs. incompatible element ratio of the volcanoes of Samaná monogenetic volcanic field and Cajamarca Complex (Blanco-Quintero et al., 2014). **(C)** Diagram of SiO_2 vs. CaO/Al_2O_3 to determine fractionation of Ca-rich minerals (plagioclase and clinopyroxene). The arrow indicates the increase in the degree of fractionation to these phases in different volcanoes. **(D,E)** Diagrams of SiO_2 vs. compatible element ratio. The arrow indicates the increase in the degree of fractionation. **(F)** Diagram of SiO_2 vs. Eu/Eu* to determine Eu anomalies. Eu/Eu* = (EuN/ $\sqrt{}$(SmN x GdN)), and the values are normalized to the chondrite value of Nakamura (1974). Abbreviations: (FC), fractional crystallization.

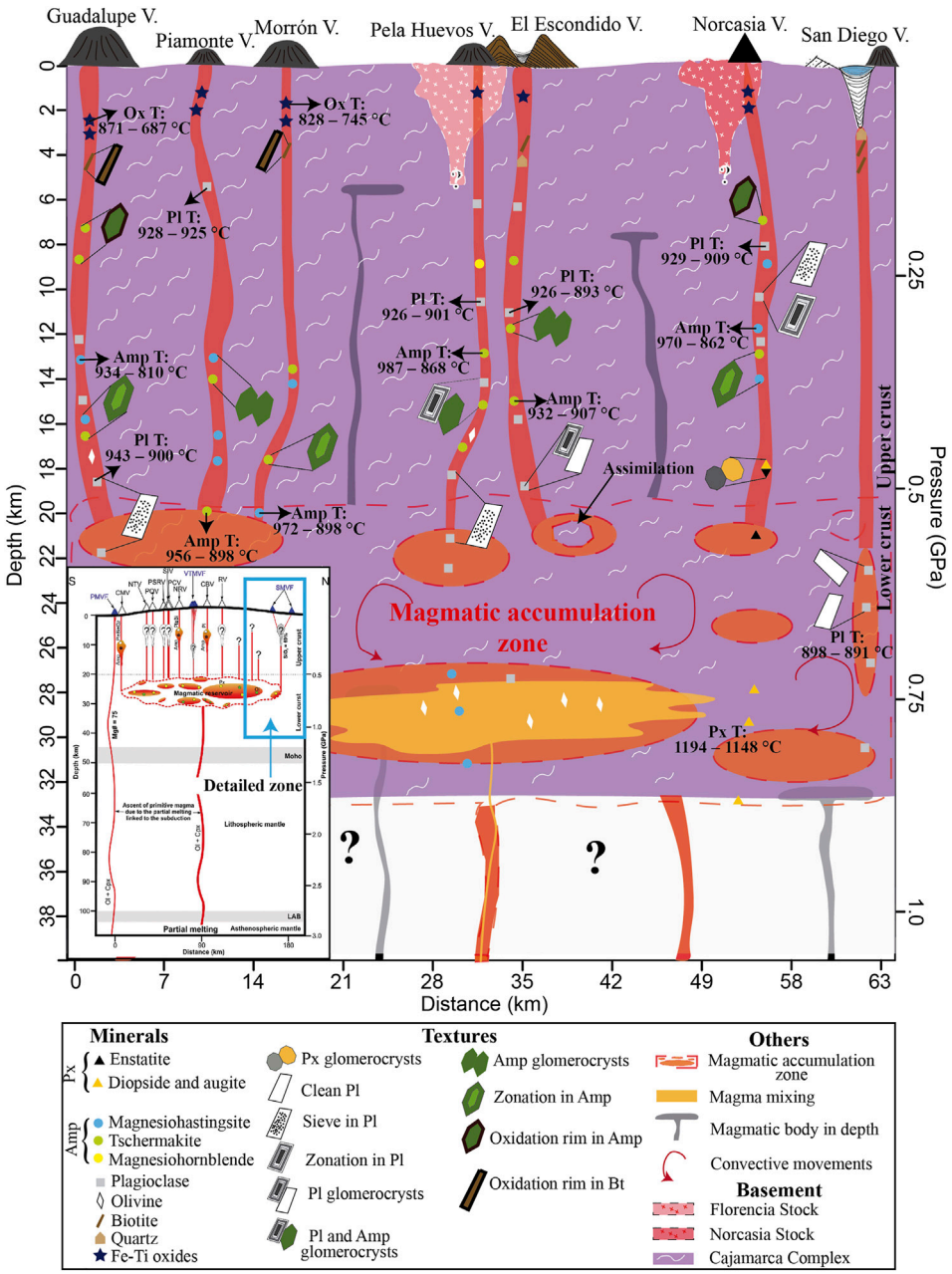

FIGURE 11 | Samaná monogenetic volcanic field magma evolution model. The depth at which the different mineral phases were formed is obtained by the equation h = [P/(ρ × g)] (White, 2013). Extrapolated depth of the Cajamarca Complex at 6,5 °N (Ureña & Mejía, 2019). In the lower left part, the San Diego—Cerro Machín Volcano-Tectonic Province model is observed (from Murcia et al., 2019), where the blue box represents the zone which this model has proposed.

consistent with processes of magma recharge that triggered magma mixing. Moreover, the reverse-zoned amphibole crystals in most of the volcanoes of the SMVF (El Escondido, Pela Huevos, Guadalupe, Norcasia and Morrón) indicate compositional variations that reveal an increase in the temperature from the core to rim (from 917 to 958°C on average), which is consistent with processes of magma recharge (c.f. Sutcliffe, 1989; Andrews et al., 2008; Kiss et al., 2014). This is also supported by the similar pressures obtained for both compositional zones (0.36 and 0.49 GPa on average), which in turn indicate mixing at shallow depths (14–19 km). In summary, it is proposed that magma recharge is another process that affected the magmas that formed the SMVF volcanoes, likely at crustal levels.

5.4 Samaná Monogenetic Volcanic Field Magma Evolution Model

At least seven monogenetic volcanic edifices are part of the northernmost volcanism in the Andean chain. This volcanism is not only long-lived but also potentially active. Recognizing this volcanism is important because the area has been commonly considered non-volcanogenic linked to a flat subduction. This volcanism also sheds light onto magmatic evolution associated with evolved monogenetic volcanism, which is common, although poorly known in the literature, in other subduction zones. In addition, this study gives insights into how the magma evolution of monogenetic fields can be more complex than that given by individual batches of magma reaching the surface uninterrupted, as is normally described for monogenetic volcanic fields of more mafic compositions.

As discussed earlier, the magmatic evolution of the SMVF reveals that fractional crystallization is the major differentiation process that magmas underwent during their ascent to the surface; this fractionation took place during multiple stagnation zones as evidenced by the geothermobarometric calculations. In addition to the process of fractional crystallization, (e.g., disequilibrium textures linked to increases of temperature), magma recharge was also evidenced not only at the source but also at different stagnation levels. The interplay of these two major processes is responsible for the range of compositions displayed by the volcanoes of the SMVF. Taking this into account, we propose the following model of magma evolution: The magma that feeds the SMVF originates by the fusion of the mantle wedge, caused by the subduction of the Nazca plate under the South American plate. The magma then rises until it stagnates at crustal levels around 20–35 km depth, according to the magmatic accumulation zone proposed by Londono (2016), using geophysical methods such as regional 3D tomography of seismic velocity. This zone is also assumed to be the main magmatic supply for the SMVF volcanoes (Murcia et al., 2019). Our geothermobarometric calculations indicate that the main mineral phases in these volcanoes form at depths that coincide with this magmatic accumulation zone (**Figure 11**). Diopside and augite crystallize between 33 and 28 km, and enstatite crystallizes at 21 km, if the values are extrapolated from those obtained from Norcasia crystals. These crystals form monomineralic glomeroporphyritic texture in both Norcasia and Pela Huevos volcanoes. Plagioclase crystallization occurs between 31 and 5 km, indicating that it starts to form within the accumulation zone up to shallow levels of the crust. These crystals exhibit disequilibrium textures such as zonation and sieve crystals, which suggest convective movement and physicochemical variations within the magma during ascent. Likewise, the crystallization of amphibole starts at the magma accumulation zone (31 km) and continues up to 7 km, with magnesio-hastingsite crystallizing between 31 and 9 km, tschermakite between 31 and 7 km, and magnesio-hornblende at 9 km. The last phases to crystallize are biotite at <800°C (c.f. Castro & Dingwell, 2009), identified in the San Diego, El Escondido, Morrón, and Guadalupe volcanoes, quartz observed in El Escondido and San Diego volcanoes, and microphenocrysts of Fe–Ti oxides in all volcanoes (**Figure 11**). In addition to the described sequence of crystallization, evidence of magma recharge in the accumulation zone is also observed. For example, the incorporation of olivine antecrysts in the magmas of Pela Huevos and Guadalupe volcanoes and reverse zonation were observed in amphiboles of El Escondido, Pela Huevos, Guadalupe Norcasia, and Morrón volcanoes (**Figure 11**). Similarly, oxidation rims were observed in amphibole crystals in rocks from Piamonte, Pela Huevos, Guadalupe, and Norcasia volcanoes (**Figure 11**). After eruption, the rapid cooling produced crystallization of microlites and solidification of the melt. As evidenced in the volcanic edifices, the magma effusively reached the surface to form the Pela Huevos, Piamonte, Morrón, and Guadalupe volcanoes and explosively to form El Escondido and San Diego volcanoes, the latter associated with the presence of water on the surface (**Figure 11**).

6 CONCLUSION

- The Samaná monogenetic volcanic field comprises at least seven andesitic to dacitic with calc-alkaline affinity volcanoes, typical of subduction environments. Ages from 1.3 Ma to 17 ka suggest that the Samaná monogenetic volcanic field is long-lived and potentially active.
- Plagioclase and amphibole are the most abundant minerals. They are present in all rocks studied, with the exception of those from San Diego volcano, which does not present amphibole. Biotite appears in the sample from the San Diego volcano and in a lesser proportion in the samples from El Escondido, Morrón, and Guadalupe volcanoes. Quartz is only present in the samples from the San Diego and El Escondido volcanoes. Pyroxene (clinopyroxene and orthopyroxene) is present in the samples from the Pela Huevos and Norcasia volcanoes. Olivine is present in low proportions in the samples from the Pela Huevos and Guadalupe volcanoes. Finally, Fe–Ti oxides are present in all samples as accessory minerals.
- Based on thermobarometric analysis, magma reached the surface at temperatures lower than <700 °C. Plagioclase crystallized at 943–891 °C and 0.8–0.1 GPa; amphibole at 987–810 °C and 0.8–0.2 GPa; diopside and augite at 1,194–1,165° C and 0.9–0.7 GPa; and enstatite crystallized at 1,148 °C and 0.6 and Fe–Ti oxides crystallized at 871–687 °C.
- The evolved character of the Samaná products indicates differentiation of magma residing at the crust, and further evolution occurred mainly due to fractionation. The presence of disequilibrium textures and mineral compositions of mafic affinity indicate processes of magma mixing triggered by magma recharge at the accumulation zone.
- The depths at which the minerals were formed coincide with the magmatic accumulation zone that feeds the SCVTP. Thus, we propose that different magma batches rise from this zone to generate each of the monogenetic volcanoes that form the SMVF.
- This study highlights that the SMVF magma evolution is complex and not as simple as in the case of rapid ascents without crustal stagnations, as usually postulated for monogenetic volcanic fields.

DATA AVAILABILITY STATEMENT

The original contributions presented in the study are included in the article/**Supplementary Material**; further inquiries can be directed to the corresponding author.

AUTHOR CONTRIBUTIONS

LS-T: Conceptualization, methodology, software formal analysis, investigation, writing, and visualization. HM: Conceptualization, methodology, investigation, writing, supervision, and funding acquisition. DS-A: Conceptualization, methodology, investigation, writing, and supervision. All approved the submitted version.

FUNDING

From Universidad de Caldas, the Vicerrectoria de Investigaciones y Posgrados provided funds through a project to HM (code 0391820) for K/Ar geochronological analyses. The mineral chemistry analyses were provided by Earth Observatory of Singapore, Nanyang Technological University, Singapore. DS-A was sponsored by MINCIENCIAS Colombia (Postdoctoral Grant No. 848-2019, Code 201010028319) at the Universidad de Caldas (Code No. 807040-125-2020).

ACKNOWLEDGMENTS

This work was performed at the Instituto de Investigaciones en Estratigrafia (IIES), Universidad de Caldas. We thank the reviewers for comments that helped us improve the manuscript and the editors of this special issue for their support. Particularly, we thank the guest editor KN and the chief editor Valerio Acocella for handling the manuscript. A final English revision was performed by Michael Ort.

SUPPLEMENTARY MATERIAL

The Supplementary Material for this article can be found online at: https://www.frontiersin.org/articles/10.3389/feart.2022.880003/full#supplementary-material

REFERENCES

Andersen, D. J., and Lindsley, D. H. (1985). New (And Final) Models for the Ti- Magnetite/ilmenite Geothermobarometer and Oxygen Barometer. *Abstr. AGU 1985 Spring Meet. Eos Trans. Am. Geophys. Union* 66, 416.

Andrews, B. J., Gardner, J. E., and Housh, T. B. (2008). Repeated Recharge, Assimilation, and Hybridization in Magmas Erupted from El Chichón as Recorded by Plagioclase and Amphibole Phenocrysts. *J. Volcanol. Geotherm. Res.* 175, 415–426. doi:10.1016/j.jvolgeores.2008.02.017

Bacon, C. R., and Hirschman, M. M. (1988). Mg/Mn Partitioning as a Test for Equilibrium between Coexisting Fe-Ti Oxides. *Am. Mineralogist* 73, 57–61.

Barrero, D., and Vesga, C. J. (1976). *Mapa geológico del Cuadrángulo K-9 Armero y mitad sur del Cuadrángulo J-9 La Dorada. Escala 1:100.000.* Bogotá: INGEOMINAS.

Bas, M. J. L., Maitre, R. W. L., Streckeisen, A., and Zanettin, B. (1986). A Chemical Classification of Volcanic Rocks Based on the Total Alkali-Silica Diagram. *J. Petrology* 27, 745–750. doi:10.1093/petrology/27.3.745

Berlo, K., Blundy, J., Turner, S., and Hawkesworth, C. (2007). Textural and Chemical Variation in Plagioclase Phenocrysts from 1980 Eruptions of Mount St. Helens, USA. *Contributions Mineralogy Petrology* 89, 1–16. doi:10.1007/s00410-007-0194-8

Best, M. G. (2003). *Igneous and Metamorphic Petrology*. Second Edition. Oxford: Blackell Science Ltd, 758p.

Blanco-Quintero, I. F., García-Casco, A., Toro, L. M., Moreno, M., Ruiz, E. C., Vinasco, C. J., et al. (2014). Late Jurassic Terrane Collision in the Northwestern Margin of Gondwana (Cajamarca Complex, Eastern Flank of the Central Cordillera, Colombia). *Int. Geol. Rev.* 56, 1852–1872. doi:10.1080/00206814.2014.963710

Blundy, J. D., and Wood, B. J. (1991). Crystal-chemical Controls on the Partitioning of Sr and Ba between Plagioclase Feldspar, Silicate Melts, and Hydrothermal Solutions. *Geochimica Cosmochimica Acta* 55, 193–209. doi:10.1016/0016-7037(91)90411-w

Bohórquez, O. P., Monsalve, M. L., Velandia, F., Gil, F., and Mora, H. (2005). Marco tectónico de la cadena volcánica más septentrional de la Cordillera Central de Colombia. *Bol. Geol.* 27, 55–79.

Boivin, P., and Thouret, J.-C. (2014). "The Volcanic Chaîne des Puys: A Unique Collection of Simple and Compound Monogenetic Edifices," in *Landscapes and Landform of France*. Editors M. Fort and M.F. André (Netherlands: Dordrecht: Springer), 81–91. doi:10.1007/978-94-007-7022-5_9

Borrero, C., Murcia, H., Agustín-Flores, J., Arboleda, M. T., and Giraldo, A. M. (2017). Pyroclastic Deposits of San Diego Maar, Central Colombia: an Example of a Silicic Magma-Related Monogenetic Eruption in a Hard Substrate. *Geol. Soc. Lond. Spec. Publ.* 446, 361–374. doi:10.1144/sp446.10

Cañón-Tapia, E. (2016). Reappraisal of the Significance of Volcanic Fields. *J. Volcanol. Geotherm. Res.* 310, 26–38. doi:10.1016/j.jvolgeores.2015.11.010

Carmichael, I. S. (1967). The Iron-Titanium Oxides of Salic Volcanic Rocks and Their Associated Ferromagnesian Silicates. *Contributions Mineralogy Petrology* 14, 36–64.

Castro, J. M., and Dingwell, D. B. (2009). Rapid Ascent of Rhyolitic Magma at Chaitén Volcano, Chile. *Nature* 461, 780–783. doi:10.1038/nature08458

Cavell, D. E. (2020). Petrogenesis of Colombian Arc Volcanoes: A Regional Study, Doctoral dissertations. Birmingham: University of Birmingham, 418p.

Cediel, F., Shaw, R. P., and Cáceres, C. (2003). "Tectonic Assembly of the Northern Andean Block," in *Volcanic and Tectonic Hazard Assessment for Nuclear Facilities*. Editors C. Bartolini, N. A. Champman, and L. J. Connor, 346–368. doi:10.1306/m79877c37

Cortés, M., Angelier, J., and Colletta, B. (2005). Paleostress Evolution of the Northern Andes (Eastern Cordillera of Colombia): Implications on Plate Kinematics of the South Caribbean Region. *Tectonics* 24 (1). doi:10.1029/2003tc001551

Davidson, J. P., Ferguson, K. M., Colucci, M. T., and Dungan, M. A. (1988). The Origin and Evolution of Magmas from the San Pedro-Pellado Volcanic Complex, S. Chile: Multicomponent Sources and Open System Evolution. *Contr. Mineral. Pet.* 100, 429–445. doi:10.1007/bf00371373

Feeley, T. C., and Sharp, Z. D. (1996). Chemical and Hydrogen Isotope Evidence for *In Situ* Dehydrogenation of Biotite in Silicic Magma Chambers. *Geol* 24, 1021–1024. doi:10.1130/0091-7613(1996)024<1021:cahief>2.3.co;2

Foster, M. D. (1960). Interpretation if the Composition of Trioctahedral Micas. *U. S. Geol. Surv. Prof. Pap.* 354-B, 1–49.

Gill, J. B. (1981). *Orogenic Andesites and Plate Tectonics*. Berlín: Springer, 370p.

Gómez-Tapias, J., Nivia, A., Montes, N. E., Almanza, M. F., Alcárcel, F. A., and Madrid, C. A. (2015). "Notas explicativas: Mapa Geológico de Colombia," in *Compilando la geología de Colombia: Una visión a 2015*. Editors J. Gómez-

Tapias and M.F. Almanza (Bogotá: Servicio Geológico Colombiano, Publicaciones Geológicas, Especiales), 9–33.

González, P. (2008). "Textura de los cuerpos ígneos," in *Geología de los cuerpos ígneos. Asociación Geológica Argentina. Serie B: Didáctica y complementaria*. Editors E.J. Llambías and J. D'Eramo (Salta, Argentina: Facultad de Ciencias Naturales, Universidad Nacional de Salta), 171–197.

Green, T. H. (1980). Island Arc and Continent-Building Magmatism - A Review of Petrogenic Models Based on Experimental Petrology and Geochemistry. *Tectonophysics* 63, 367–385. doi:10.1016/0040-1951(80)90121-3

Groove, T. L., and Till, C. B. (2015). "Melting the Earth´s Upper Mantle," in *Encyclopedia of Volcanoes*. Editors H. Sigurdsson, B. Houghton, S. R. McNutt, H. Rymer, and J. Stix. 2nd edition (El Sevier, USA: Academic Prees), 35–47.

Hogan, J. P. (1993). Monomineralic Glomerocrysts: Textural Evidence for Mineral Resorption during Crystallization of Igneous Rocks. *J. Geol.* 101, 531–540. doi:10.1086/648245

Idárraga-García, J., Kendall, J.-M., and Vargas, C. A. (2016). Shear Wave Anisotropy in Northwestern South America and its Link to the Caribbean and Nazca Subduction Geodynamics. *Geochem. Geophys. Geosyst.* 17, 3655–3673. doi:10.1002/2016gc006323

Jeffery, A. J., Gertisser, R., Troll, V. R., Jolis, E. M., Dahren, B., Harris, C., et al. (2013). The Pre-eruptive Magma Plumbing System of the 2007-2008 Dome-Forming Eruption of Kelut Volcano, East Java, Indonesia. *Contrib. Mineral. Pet.* 166, 275–308. doi:10.1007/s00410-013-0875-4

Jerram, D. A., and Martin, V. M. (2008). "Understanding Crystal Populations and Their Significance through the Magma Plumbing System," in *Geological Society*. Editors C. Annen and G.F. Zellmer (London: Special Publications), 133–148. doi:10.1144/sp304.7

Kiss, B., Harangi, S., Ntaflos, T., Mason, P. R. D., and Pál-Molnár, E. (2014). Amphibole Perspective to Unravel Pre-eruptive Processes and Conditions in Volcanic Plumbing Systems beneath Intermediate Arc Volcanoes: a Case Study from Ciomadul Volcano (SE Carpathians). *Contrib. Mineral. Pet.* 167, 986. doi:10.1007/s00410-014-0986-6

Leake, B. E., Woolley, A. R., Arps, C. E. S., Birch, W. D., Gilbert, M. C., Grice, J. D., et al. (1997). Nomenclature of Amphiboles; Report of the Subcommittee on Amphiboles of the International Mineralogical Association Commission on New Minerals and Mineral Names. *Mineral. Mag.* 61, 295–310. doi:10.1180/minmag.1997.061.405.13

Lepage, L. D. (2003). ILMAT: an Excel Worksheet for Ilmenite-Magnetite Geothermometry and Geobarometry. *Comput. Geosciences* 29, 673–678. doi:10.1016/s0098-3004(03)00042-6

Londono, J. M. (2016). Evidence of recent deep magmatic activity at Cerro Bravo-Cerro Machín volcanic complex, central Colombia. Implications for future volcanic activity at Nevado del Ruiz, Cerro Machín and other volcanoes. *J. Volcanol. Geotherm. Res.* 324, 156–168. doi:10.1016/j.jvolgeores.2016.06.003

Londoño, J. M., Vallejo, K., and Quintero, S. (2020). Detailed seismic velocity structure of the Caribbean and Nazca Plates beneath Valle Medio del Magdalena region of Ne Colombia. *J. S. Am. Earth Sci.* 103, 102762. doi:10.1016/j.jsames.2020.102762

Lonsdale, P. (2005). Creation of the Cocos and Nazca Plates by Fission of the Farallon Plate. *Tectonophysics* 404, 237–264. doi:10.1016/j.tecto.2005.05.011

Loomis, T. P. (1982). Numerical Simulations of Crystallization Processes of Plagioclase in Complex Melts: the Origin of Major and Oscillatory Zoning in Plagioclase. *Contr. Mineral. Pet.* 81, 219–229. doi:10.1007/bf00371299

Lucassen, F., Becchio, R., Harmon, R., Kasemann, S., Franz, G., Trumbull, R., et al. (2001). Composition and Density Model of the Continental Crust at an Active Continental Margin-The Central Andes between 21° and 27°S. *Tectonophysics* 341, 195–223. doi:10.1016/s0040-1951(01)00188-3

McGee, L. E., and Smith, I. E. M. (2016). Interpreting Chemical Compositions of Small Scale Basaltic Systems: a Review. *J. Volcanol. Geotherm. Res.* 325, 45–60. doi:10.1016/j.jvolgeores.2016.06.007

Monfaredi, B., Masoudi, F., Tabakh, S. A., Shaker, A. F., and Halama, R. (2009). Magmatic Interaction as Recorded in Texture and Composition of Plagioclase Phenocrysts from the Sirjan Area, Urumieh-Dokthar Magmatic Arc, Iran. *J. Sci. Islamic Repub. Iran* 20, 243–251.

Monsalve, M. L., Ortiz, I. D., and Norini, G. (2019). El Escondido, a Newly Identified Silicic Quaternary Volcano in the NE Region of the Northern Volcanic Segment (Central Cordillera of Colombia). *J. Volcanol. Geotherm. Res.* 383, 47–62. doi:10.1016/j.jvolgeores.2017.12.010

Monsalve–Bustamante, M. L. (2020). "The Volcanic Front in Colombia: Segmentation and Recent and Historical Activity," in *The Geology of Colombia, Volume 4 Quaternary*. Editors J. Gómez and A. O. Pinilla–Pachon (Bogotá: Servicio Geológico Colombiano, Publicaciones Geológicas Especiales), 97–159. doi:10.32685/pub.esp.38.2019.03

Mora, J. A., Oncken, O., Le Breton, E., Ibánez-Mejia, M., Faccenna, C., Veloza, G., et al. (2017). Linking Late Cretaceous to Eocene Tectonostratigraphy of the San Jacinto Fold Belt of NW Colombia with Caribbean Plateau Collision and Flat Subduction. *Tectonics* 36, 2599–2629. doi:10.1002/2017tc004612

Morimoto, N. (1989). Nomenclature of Pyroxenes. *Mineralogical J.* 14, 198–221. doi:10.2465/minerj.14.198

Murcia, H., Borrero, C., and Németh, K. (2019). Overview and Plumbing System Implications of Monogenetic Volcanism in the Northernmost Andes' Volcanic Province. *J. Volcanol. Geotherm. Res.* 383, 77–87. doi:10.1016/j.jvolgeores.2018.06.013

Murcia, H., and Németh, K. (2020). "Effusive Monogenetic Volcanism," in *Volcanoes-Updates in Volcanology* (London, UK: IntechOpen).

Nakamura, N. (1974). Determination of REE, Ba, Fe, Mg, Na and K in Carbonaceous and Ordinary Chondrites. *Geochimica Cosmochimica Acta* 38, 757–775. doi:10.1016/0016-7037(74)90149-5

Nelson, S. T., and Montana, A. (1992). Sieve Textured Plagioclase in Volcanic Rocks Produced by Rapid Decompression. *Am. Mineralogist* 77, 1242–1249.

Németh, K. (2010). Monogenetic Volcanic Fields: Origin, Sedimentary Record, and Relationship with Polygenetic Volcanism. *Special Pap. Geol. Soc. Am.* 470, 43–66. doi:10.1130/2010.2470(04)

Parat, F., Dungan, M. A., and Lipman, P. W. (2005). Contemporaneous Trachyandesitic and Calc-Alkaline Volcanism of the Huerto Andesite, San Juan Volcanic Field, Colorado, USA. *J. Petrology* 46, 589–891. doi:10.1093/petrology/egi003

Pearce, J. A., and Norry, M. J. (1979). Petrogenetic Implications of Ti, Zr, Y, and Nb Variations in Volcanic Rocks. *Contr. Mineral. Pet.* 69, 33–47. doi:10.1007/bf00375192

Pearce, J. A. (1983). "Role of the Sub-continental Lithosphere in Magma Genesis at Active Continental Margins," in *Continental Basalts and Mantle Xenoliths*. Editors C. Hawkesworth and M. Norry (Nantwich, Cheshire, England: Shiva Publication), 230–249.

Pearce, T., and Kolisnik, A. (1990). Observations of Plagioclase Zoning Using Interference Imaging. *Earth-Science Rev.* 29, 9–26. doi:10.1016/0012-8252(0)90024-p

Peccerillo, A., and Taylor, S. R. (1976). Geochemistry of Eocene Calc-Alkaline Volcanic Rocks from the Kastamonu Area, Northern Turkey. *Contr. Mineral. Pet.* 58, 63–81. doi:10.1007/bf00384745

Pennington, W. D. (1981). Subduction of the Eastern Panama Basin and Seismotectonics of Northwestern South America. *J. Geophys. Res.* 86, 10753–10770. doi:10.1029/jb086ib11p10753

Putirka, K. D. (2008). Thermometers and Barometers for Volcanic Systems. *Rev. Mineralogy Geochem.* 69, 61–120. doi:10.2138/rmg.2008.69.3

Rahman, S., and MacKenzie, W. S. (1969). The Crystallization of Ternary Feldspars: a Study from Natural Rocks. *Am. Mineralogy J. Sci.* 267, 391–406.

Rapprich, V., Shields, S., Haladova, P., Lindline, J., De Vries, B. V. W., Petronis, M. S., et al. (2017). Fingerprints of Magma Mingling Processes within the Miocene Zebin Tuff Cone Feeding System (Jicin Volcanic Field, Czech Republich). *J. Geosciences* 62, 215–229. doi:10.3190/jgeosci.245

Ridolfi, F., Puerini, M., Renzulli, A., Menna, M., and Toulkeridis, T. (2008). The Magmatic Feeding System of El Reventador Volcano (Sub-andean Zone, Ecuador) Constrained by Texture, Mineralogy and Thermobarometry of the 2002 Erupted Products. *J. Volcanol. Geotherm. Res.* 176, 94–106. doi:10.1016/j.jvolgeores.2008.03.003

Ridolfi, F., and Renzulli, A. (2012). Calcic Amphiboles in Calc-Alkaline and Alkaline Magmas: Thermobarometric and Chemometric Empirical Equations Valid up to 1,130°C and 2.2 GPa. *Contrib. Mineral. Pet.* 163, 877–895. doi:10.1007/s00410-011-0704-6

Ridolfi, F., Renzulli, A., and Puerini, M. (2010). Stability and Chemical Equilibrium of Amphibole in Calc-Alkaline Magmas: an Overview, New Thermobarometric Formulations and Application to Subduction-Related Volcanoes. *Contrib. Mineral. Pet.* 160, 45–66. doi:10.1007/s00410-009-0465-7

Rollinson, H. R. (1993). *Using Geochemical Data: Evaluation, Presentation, Interpretation*. Harlow, Essex, England: Routledge, 352p.

Romick, J. D., Kay, S. M., and Kay, R. W. (1992). The Influence of Amphibole Fractionation on the Evolution of Calc-Alkaline Andesite and Dacite Tephra from the Central Aleutians, Alaska. *Contrib. Mineral. Pet.* 112, 101–118. doi:10.1007/bf00310958

Rueda-Gutiérrez, J. B. (2019). Aportes al conocimiento del Magmatismo de la Cordillera Central de Colombia en su Flanco Oriental: Área geotérmica de San Diego, Samaná, Caldas. *Bol. Geol.* 41, 45–70. doi:10.18273/revbol.v41n2-2019003

Rutherford, M. J., and Hill, P. M. (1993). Magma Ascent Rates from Amphibole Breakdown: An Experimental Study Applied to the 1980-1986 Mount St. Helens Eruptions. *J. Geophys. Res.* 98, 19667–19685. doi:10.1029/93jb01613

Salazar-Muñoz, N., Ríos, C. A., Murcia, H., Schonwalder-Ángel, D., Botero-Gómez, L. A., Hincapié, G., et al. (2021). Andesitic (SiO2: ~ 60 Wt%) Monogenetic Volcanism in the Northern Colombian Andes: Crystallisation History of Three Quaternary Volcanoes. *J. Volcanol. Geotherm. Res.* 412, 107194. doi:10.1016/j.jvolgeores.2021.107194

Sánchez-Torres, L., Toro, A., Murcia, H., Borrero, C., Delgado, R., and Gómez-Arango, J. (2019). El Escondido Tuff Cone (38 Ka): a Hidden History of Monogenetic Eruptions in the Northernmost Volcanic Chain in the Colombian Andes. *Bull. Volcanol.* 81, 71. doi:10.1007/s00445-019-1337-2

Sen, G. (2014). *Petrology*. Berlin: Springer, 371p.

Shcherbakov, V. D., Plechov, P. Y., Izbekov, P. E., and Shipman, J. S. (2010). Plagioclase Zoning as an Indicator of Magma Processes at Bezymianny Volcano, Kamchatka. *Contrib. Mineral. Pet.* 162, 83–99. doi:10.1007/s00410-010-0584-1

Smith, I. E. M., and Németh, K. (2017). Source to Surface Model of Monogenetic Volcanism: a Critical Review. *Geol. Soc. Lond. Spec. Publ.* 446, 1–28. doi:10.1144/sp446.14

Sosa-Ceballos, G., Boijseauneau-López, M. E., Pérez-Orozco, J. D., Cifuentes-Nava, G., Bolós, X., Perton, M., et al. (2021). Silicic Magmas in the Michoacán-Guanajuato Volcanic Field: an Overview about Plumbing Systems, Crustal Storage and Genesis Processes. *revmexcg* 38, 210–225. doi:10.22201/cgeo.20072902e.2021.3.1668

Stormer, J. C. (1983). The Effects of Recalculation on Estimates of Temperature and Oxygen Fugacity from Analyses of Multicomponent Iron-Titanium Oxides. *Am. Mineralogist* 68, 586–594.

Sun, S.-s., and McDonough, W. F. (1989). Chemical and Isotopic Systematics of Oceanic Basalts: Implications for Mantle Composition and Processes. *Geol. Soc. Lond. Spec. Publ.* 42, 313–345. doi:10.1144/gsl.sp.1989.042.01.19

Sutcliffe, R. H. (1989). Magma mixing in late Archean tonalitic and mafic rocks of the Lac des Iles area, western Superior province. *Precambrian Res.* 44, 81–101. doi:10.1016/0301-9268(89)90077-6

Suter, F., Sartori, M., Neuwerth, R., and Gorin, G. (2008). Structural Imprints at the Front of the Chocó-Panamá Indenter: Field Data from the North Cauca Valley Basin, Central Colombia. *Tectonophysics* 460, 134–157. doi:10.1016/j.tecto.2008.07.015

Syracuse, E. M., Maceira, M., Prieto, G. A., Zhang, H., and Ammon, C. J. (2016). Multiple Plates Subducting beneath Colombia, as Illuminated by Seismicity and Velocity from the Joint Inversion of Seismic and Gravity Data. *Earth Planet. Sci. Lett.* 444, 139–149. doi:10.1016/j.epsl.2016.03.050

Taboada, A., Rivera, L. A., Fuenzalida, A., Cisternas, A., Philip, H., Bijwaard, H., et al. (2000). Geodynamics of the Northern Andes: Subductions and Intracontinental Deformation (Colombia). *Tectonics* 19, 787–813. doi:10.1029/2000tc900004

Tsuchiyama, A. (1985). Dissolution Kinetics of Plagioclase in the Melt of the System Diopside-Albite-Anorthite, and Origin of Dusty Plagioclase in Andesites. *Contr. Mineral. Pet.* 89, 1–16. doi:10.1007/bf01177585

Ureña, M. A., and Mejía, M. (2019). Estructura interna del Batolito Antioqueño y cuerpos intrusivos aledaños a partir de tomografía sísmica 3D de velocidad, Bachelor thesis. Colombia: University of Caldas, 114p.

Valentine, G. A., and Gregg, T. K. P. (2008). Continental Basaltic Volcanoes - Processes and Problems. *J. Volcanol. Geotherm. Res.* 177, 857–873. doi:10.1016/j.jvolgeores.2008.01.050

Valentine, G. A., Ort, M. H., and Cortés, J. A. (2021). Quaternary Basaltic Volcanic Fields of the American Southwest. *Geosphere* 17, 2144–2171. doi:10.1130/ges02405.1

Vargas, C. A., and Mann, P. (2013). Tearing and Breaking off of Subducted Slabs as the Result of Collision of the Panama Arc-Indenter with Northwestern South America. *Bull. Seismol. Soc. Am.* 103, 2025–2046. doi:10.1785/0120120328

Varol, E., Temel, A., Yürür, T., Gourgaud, A., and Bellon, H. (2014). Petrogenesis of the Neogene Bimodal Magmatism of the Galatean Volcanic Province, Central Anatolia, Turkey. *J. Volcanol. Geotherm. Res.* 280, 14–29. doi:10.1016/j.jvolgeores.2014.04.014

Varol, E., Ternel, A., and Gourgaud, A. (2008). Textural and Compositional Evidence for Magma Mixing in the Evolution of the Camlidere Volcanic Rocks (Galatean Volcanic Province), Central Anatolia, Turkey. *Turkish J. Earth Sci.* 17, 709–727. doi:10.3906/yer-0703-8

Velandia, J., Murcia, H., Németh, K., and Borrero, C. (2021). Uncommon Mafic Rocks (MgO> 10 wt.%) in the Northernmost Andean Volcanic Chain (4°25′N): Implications for Magma Source and Evolution. *J. S. Am. Earth Sci.* 110, 103308. doi:10.1016/j.jsames.2021.103308

Viccaro, M., Giacomoni, P. P., Ferlito, C., and Cristofolini, R. (2010). Dynamics of Magma Supply at Mt. Etna Volcano (Southern Italy) as Revealed by Textural and Compositional Features of Plagioclase Phenocrysts. *Lithos* 116, 77–91. doi:10.1016/j.lithos.2009.12.012

Viccaro, M., Giuffrida, M., Nicotra, E., and Ozerov, A. Y. (2012). Magma Storage, Ascent and Recharge History Prior to the 1991 Eruption at Avachinsky Volcano, Kamchatka, Russia: Inferences on the Plumbing System Geometry. *Lithos* 140-141, 11–24. doi:10.1016/j.lithos.2012.01.019

Villagómez, D., Spikings, R., Magna, T., Kammer, A., Winkler, W., and Beltrán, A. (2011). Geochronology, Geochemistry and Tectonic Evolution of the Western and Central Cordilleras of Colombia. *Lithos* 125, 875–896. doi:10.1016/j.lithos.2011.05.003

Wagner, L. S., Jaramillo, J. S., Ramírez-Hoyos, L. F., Monsalve, G., Cardona, A., and Becker, T. W. (2017). Transient Slab Flattening beneath Colombia. *Geophys. Res. Lett.* 44, 6616–6623. doi:10.1002/2017gl073981

White, W. M. (2013). *Geochemistry*. first edition. New Jersey: John Wiley & Sons, 644p.

Wilkinson, J. F. G., and Taylor, S. R. (1981). Trace Element Fractionation Trends of Tholeiitic Magma at Moderate Pressure: Evidence from an Al-Spinel Ultramafic-Mafic Inclusion Suite. *Contr. Mineral. Pet.* 75, 225–233. doi:10.1007/bf01166762

Williams, H. M., Nielsen, S. G., Renac, C., Griffin, W. L., O'Reilly, S. Y., McCammon, C. A., et al. (2009). Fractionation of Oxygen and Iron Isotopes by Partial Melting Processes: Implications for the Interpretation of Stable Isotope Signatures in Mafic Rocks. *Earth Planet. Sci. Lett.* 283, 156–166. doi:10.1016/j.epsl.2009.04.011

Zellmer, G. F. (2021). Gaining Acuity on Crystal Terminology in Volcanic Rocks. *Bull. Volcanol.* 833, 1–8. doi:10.1007/s00445-021-01505-9

Conflict of Interest: The authors declare that the research was conducted in the absence of any commercial or financial relationships that could be construed as a potential conflict of interest.